energies

MDPI

Review

Scaling Performance Parameters of Reciprocating Engines for Sustainable Energy System Optimization Modelling

Ward Suijs [1] and Sebastian Verhelst [1,2,*]

[1] Department of Electromechanical, Systems and Metal Engineering, Ghent University, Sint-Pietersnieuwstraat 41, 9000 Ghent, Belgium; ward.suijs@ugent.be
[2] Department of Energy Sciences, Lund University, Ole Römers väg 1, Box 118, SE-221 00 Lund, Sweden
* Correspondence: sebastian.verhelst@ugent.be

Abstract: The increased share of variable renewable energy sources such as wind and solar power poses constraints on the stability of the grid and the security of supply due to the imbalance between electricity production and demand. Chemical storage or power-to-X technologies can provide the flexibility that is needed to overcome this issue. To quantify the needs of such storage systems, energy system optimization models (ESOMs) are used, guiding policy makers in nationwide energy planning. The key input parameters for such models are the capacity and efficiency values of the conversion devices. Gas turbines, reciprocating engines, fuel cells and Rankine engines are often mentioned here as cogeneration technologies. Their performance parameters will however need to be revised when switching from fossil to renewable fuels. This study therefore investigates the possibility of using size-based scaling laws to predict the efficiency and power values of one type of conversion technology: the reciprocating engine. The most straightforward scaling laws are the ones based on the fundamental engine performance parameters and are constructed by fitting an arithmetic function for a large set of representative engine data. Their accuracy was tested with a case study, consisting of thirty large-bore, spark-ignited gas engines. Two alternative methods were also investigated: scaling laws based on the Willans line method and scaling laws based on the similarity theory. Their use is deemed impractical for the current research problem.

Keywords: energy system; energy storage; power-to-X; synthetic fuels; electrofuels; scaling laws; ICE; Willans line; similarity; spark ignition

Citation: Suijs, W.; Verhelst, S. Scaling Performance Parameters of Reciprocating Engines for Sustainable Energy System Optimization Modelling. *Energies* **2023**, *16*, 7497. https://doi.org/10.3390/en16227497

Academic Editors: Daniela Anna Misul and Mirko Baratta

Received: 11 October 2023
Revised: 30 October 2023
Accepted: 7 November 2023
Published: 8 November 2023

1. Introduction

A high penetration of renewable energy systems such as wind and solar energy will need to be accompanied by additional renewable energy buffers to overcome the mismatch between electricity demand and electricity supply [1]. This cooperative synergy between variable renewable energy sources (VRES) and other energy sources is being thoroughly investigated in hybrid renewable energy systems (HRES) [2,3]. The integration of large-scale energy storage devices (ESDs) into these systems is imminent [4]. A forecast of global electricity generation in 2040 estimates that major markets such as the United States would need an installed storage capacity of 470 GWh if they have more than 40% VRES, while China would need more than 600 GWh [5]. Similarly, in Europe, a fully renewable electricity landscape would require a storage capacity of around 100–300 TWh under an optimal renewable energy mix [6–8]. In this regard, chemical storage or power-to-X technologies can provide the flexibility that is needed with new capacity investments in VRES [9]. In power-to-X, CO_2 and H_2O are combined with a surplus of renewable electricity to produce synthetic versions of various fuels (e.g., methane, methanol, ammonia), all with green hydrogen as the basic building block. Considering the way these fuels are produced, they are also called 'electrofuels' or 'e-fuels'. The remaining uncertainties are the quantities that will be needed in the future (as a function of the renewable shares) and their associated

costs [10]. Rixhon et al. [11] stated that in order to realize the maximum potential of these synthetic energy carriers in a sustainable transition, it will be necessary to study the integration of these electrofuels within a multi-sector and whole-energy system. This can be achieved using energy system optimization models (ESOMs). These optimization models can be used to find the cost-optimal combination of fuels and conversion technologies to meet the energy demand [12]. They are considered to be very robust due to their detailed implementation of the techno-economic, spatial and environmental characteristics of the power system [13]. As a result, these optimization models have been used extensively in the last decade to analyze national policies [12]. For example, Sparatu et al. [14] used a spreadsheet tool to present two alternative scenarios for meeting the UK's energy system decarbonization ambitions, one of which focused on developing VRES with energy storage and nuclear power. Aboumahboub et al. [15] used an open-source energy modelling system (OSeMOSYS) to explore the possibility of investing heavily in solar PV and energy storage technologies to decarbonize Australia's energy system and meet the 1.5 °C climate goals according to the Paris agreement. Finally, Limpens et al. [16] analyzed the Belgian energy system in 2035 for different carbon emission targets through a multi-objective optimization approach using the open-source Energy TD model. In their study, they used an hourly time step in order to make the model suitable for analyzing the integration of intermittent renewables and storage.

One of the three entities that make up an ESOM are the technologies that convert energy carriers from one form to another [17]. The key input parameters for the model are the techno-economic parameters of these conversion technologies, of which efficiency, lifetime, operating range and maintenance performance are the most important ones. A specific type of conversion device is the prime mover in cogeneration and trigeneration systems. Cogeneration or combined heat and power (CHP) systems use the energy in the fuel to simultaneously produce electricity and useful heat. Trigeneration or combined cooling, heating and power (CCHP) systems add another level of complexity by producing a cooling stream in addition to electricity and heat [18,19]. Jradi et al. [20] compared the electrical efficiencies and power ratings of the four prime movers used for electricity generation: gas turbines, internal combustion engines (ICEs), fuel cells and Rankine engines. For fossil-fueled plants, the results are as follows: gas turbines tend to have electrical efficiency values of 18–36%, with plant capacities of up to 250 MW. Similar values are found for Rankine engines (15–38%) for the same power output. ICEs are the most commonly used prime mover in the medium-scale CHP and CCHP application range [21], achieving electrical efficiencies of between 25–45% with cogeneration capacities of up to 75 MW. The highest electrical efficiencies can be achieved by using fuel cells, where values of 37–60% can be found, but at lower plant capacities, up to 2 MW is possible.

These current values will need to be revised because the properties of synthetic fuels can differ significantly from conventional fuels such as gasoline, diesel and natural gas [22]. Updated values are needed for a wide span of applications, implementing the conversion devices at the neighborhood, district and city levels [23]. Therefore, this work investigates the existence and use of size-based scaling laws to quantify the performance parameters of prime movers and, more specifically, the internal combustion engine running on alternative fuels. The purpose of these scaling laws is to predict key operating conditions, such as the peak brake thermal efficiency (BTE) and peak brake power output, solely on the basis of the required size of the engine, disregarding other operating characteristics for the time being. This is in steep contrast with conventional engine performance prediction models, where, with different levels of complexity, thermodynamics laws for mass and energy conservation are implemented [24–27]. Even though these scaling laws are not able to accurately reproduce the sensitivities to the other operating characteristics (e.g., operating speed, injection timing, spark timing, air-to-fuel ratio) of the engine, given the inaccuracies that arise within the energy system optimization models when predicting future events [11,28], they may represent a viable compromise between computational cost and accuracy.

The focus of this work is on the scaling laws for spark-ignition (SI) engines. The electrofuels most likely to reach a certain level of cost-competitiveness (e.g., hydrogen, methanol, methane and ammonia) tend more toward spark-ignition operation than to their compression-ignition (CI) counterpart [29–33]. However, as there has been less interest in large-bore SI engines in the past, and the scaling laws for general ICEs and CI engines are also examined. This review paper is divided into two main parts, the first part is based on the most accessible type of scaling laws: curve-fitted equations. The second part consists of two alternative methods that have been found, the Willans line method and the similitude approach. The first part is structured as follows: Section 2.1 is a summary of map-based, curve-fitted scaling laws. Since this type of scaling law requires a large data set for high accuracy, the constructed equations are rarely only based on SI data, and the resulting scaling laws are valid for both SI/CI four-stroke engines. The predicted performance parameters are the torque, brake engine power and brake thermal efficiency. In Section 2.2, a literature review of large-bore heavy-duty SI engines running on synthetic fuels is added, as they will have to provide the necessary input data required to apply this method to the current research problem. The first part is then concluded in Section 2.3, where a case study evaluates the performance of the curve-fitted scaling laws on a data set consisting of large-bore, prechamber SI natural gas engines. The second part consists of Sections 3.1 and 3.2. Section 3.1 examines the possibility of using the Willans line method to scale the engine performance. The Willans line method assumes that, at a constant engine speed, the fuel consumption and power output can be scaled quasi-linearly. Section 3.2 also considers the applicability of similitude.

With the help of this overview of scaling laws, an optimal method can be chosen to provide more accurate input data (capacity and efficiency of the ICE as a conversion device) to ESOMs with little additional computational costs.

2. Curve-Fitted Equations

2.1. Scaling Laws

The most simple way to predict the relationship between any combination of two or more variables is to construct an empirical curve that best fits a set of data points. This approach results in data-driven equations, excluding the influence of some or all physics-based parameters. The quality of the fit can be measured using the R^2 value, or the coefficient of determination. Its value ranges from zero to unity, and it provides a measure of how well the observed outcome is represented by the model.

Menon [34] and Brown [35] both fitted a power curve to a data set of peak power versus displacement volume for a large number of ICEs. Equation (1) shows the form of the power curve; the coefficients a and b of each correlation can be found in Table 1. To create uniformity among the different references, these coefficients have been recalculated from their source values so that the power is expressed in kW and the volume in liters (dm^3). The unit of constant 'a' then changes according to the equation in order to match the left- and right-hand sides:

$$y = a \cdot x^b \quad (1)$$

In Equation (1), the response value y is the total peak power (kW) and the variable x is the total displacement volume of the engine (dm^3). As can be seen in Table 1, both coefficients differ greatly for each data set. For an engine with a displacement volume of 10 dm^3, the power curve of Menon et al. [34] predicts a peak power value of 249 kW, while the curve of Brown et al. [35] predicts only 205 kW. Thus, the coefficients largely depend on the data set used. Menon correlated their function to a recent data set consisting of four-stroke aircraft engines, four-stroke light-duty vehicle engines, spark-ignition engines and diesel engines, all between 0.1 dm^3 and 100 dm^3. Brown's curve is based on data from McMahon and Bonner from 1983 [36]. The data set consists of small single-cylinder two-stroke gasoline engines of 0.01 dm^3 very large 16-cylinder four-stroke diesel engines of 104 dm^3. Large diesel engines typically operate under diluted conditions, reducing the specific power (kW/dm^3) of the engine. Moreover, tremendous improvements have been

made in recent decades with regard to the breathing capabilities of internal combustion engines. Four valves per cylinder have become the norm instead of two valves per cylinder, and the downsizing trend is steadily increasing the number of turbocharged cars. It is thus not a surprise that a higher specific power is predicted with a more recent set of data.

Menon used the same approach for the brake thermal efficiency [34]. For a data set consisting of both two- and four-stroke SI and diesel combustion engines, the efficiency could be predicted by a power curve of the form:

$$BTE\ [\%] = 24.644 \cdot \left(\frac{V_d}{1\ \mathrm{dm}^3} \right)^{0.0688} \tag{2}$$

where the displacement volume V_d is set in (dm^3). Since the brake thermal efficiency is already a dimensionless number, its value is much less dependent on the engine size. The exponent of Equation (2) is close to zero, while the previous two equations predicted a more linear relationship. The main reason why the efficiency continues to increase with the engine size is due to the smaller surface area to volume (SA/V_d) ratio of bigger engines [37,38]. The lower surface area simultaneously reduces heat losses and friction losses, thereby increasing the useful work of the engine. Menon [34] reported an R^2 value of 0.3316 for the efficiency correlation, meaning that only 33% of the *BTE* behavior can be explained by a variation in the displacement volume.

A more pragmatic approach for developing curve-fitted scaling laws is to start from the fundamental engine performance parameters. Chon and Heywood [39] developed four linear scaling laws to better predict torque and power as function of engine size. Based on the definition of brake mean effective pressure (*BMEP*), torque should scale with the total displacement volume as follows:

$$T\ [\mathrm{Nm}] = \frac{BMEP}{2\pi \cdot n_r \cdot 10^3} \cdot V_d \tag{3}$$

where n_r is the number of crank revolutions per cycle, *BMEP* is in Pa and the total engine displacement volume V_d is in dm^3. For a four-stroke engine, n_r equals 2. For a given engine design and technology, BMEP should be relatively constant and hence the correlation should be linear.

In order to scale the rated power with the engine size, Equation (3) is multiplied with the angular speed at the rated operating conditions. Simplifying it results in Equation (4):

$$P_{rated}\ [\mathrm{kW}] = \frac{N_{rated} \cdot BMEP_{P_{rated}}}{6 \cdot 10^7 \cdot n_r} \cdot V_d \tag{4}$$

where N_{rated} (rpm) is the speed of the engine, $BMEP_{P_{rated}}$ is in Pa and V_d again is in dm^3. The slope of this line indicates the specific power of the engine in kW/dm^3 and is widely used as a reference value for engine performance. Since the engine speed is also a variable among engines of different sizes, the accuracy of this scaling law is estimated to be quite low. A better representative of speed would be to use the maximum mean piston speed, since the latter is limited by both airflow choking over the intake valves and inertia forces in large-bore pistons [40]. The maximum mean piston speed is defined by:

$$c_m \left[\frac{\mathrm{m}}{\mathrm{s}} \right] = 2 \cdot S \cdot \frac{N_{rated}}{600} \tag{5}$$

with S being the stroke of the engine (dm). Combining Equations (4) and (5) results in the third scaling law, Equation (6):

$$P_{rated}\ [\mathrm{kW}] = \frac{BMEP_{Prated} \cdot c_m}{2 \cdot 10^5 \cdot n_r} \cdot A_p \tag{6}$$

with A_p being the total piston area (dm^2) and BMEP again being in Pa.

Chon and Heywood [39] assessed the performance of the first three scaling laws on engine performance data for the 150 available spark-ignition engines in North America in 1999. They observed that, contrary to their assumption, the maximum mean piston speed still showed a large variation from the mean value. Subsequently, they proposed a fourth scaling law that correlates the rated power divided by the mean piston speed to the total piston area:

$$\frac{P_{rated}}{c_m}\left[\frac{\text{kWs}}{\text{m}}\right] = \frac{BMEP_{Prated}}{2{\cdot}10^5{\cdot}n_r}{\cdot}A_p \tag{7}$$

The relationship in Equation (7) should be approximately linear, with potential outliers being clarified through variations in the *BMEP* at the rated power among the different engine types. The coefficients obtained when fitting the data set to these four scaling laws correspond to engines featuring four valves per cylinder, naturally aspirated and with fixed valve timing. Their values can be found in Table 1. An excellent fit was achieved for the torque scaling law, as evidenced by an R^2 value of 0.9753. When predicting the rated power based on Equation (4), the results demonstrated the anticipated scaling behavior, yielding an R^2 value of 0.9357. However, it is important to highlight that certain engines deviated by more than 20% from the linear regression averages. After accounting for variance in the mean piston speed, Equation (7) exhibited a much better fit, elevating the coefficient of determination to 0.9667.

In 2009, Heywood and Welling conducted a similar analysis using available engine models in North America spanning the years from 2000 to 2008 [41]. Their data were expanded to encompass diesel and flex fuel engines, even though gasoline engines still held a dominant 90% market share. Assuming a bore-to-stroke ratio of one, they wrote out an additional correlation between engine size and power. Given that the displacement volume can be expressed as:

$$V_d\ [\text{dm}^3] = N_c{\cdot}\frac{\pi{\cdot}B^2}{4}{\cdot}S = N_c{\cdot}\frac{\pi{\cdot}S^3}{4} \tag{8}$$

where N_c is utilized to represent the number of cylinders and the stroke S is expressed in dm to derive the volume in liters. Combining Equations (4), (5) and (8) results in:

$$P_{rated}\ [\text{kW}] = 0.23{\cdot}10^{-5}{\cdot}BMEP_{P_{rated}}{\cdot}c_m{\cdot}V_d^{\frac{2}{3}}{\cdot}N_c^{\frac{1}{3}} \tag{9}$$

where again, under the assumption that the *BMEP* and the maximum mean piston speed of engines within the same class remain relatively constant, the scaling of rated power should correspond to $(V_d^{\frac{2}{3}}{\cdot}N_c^{\frac{1}{3}})$.

In contrast with previous research, Rowton et al. [42] approached their study on scaling laws from a different perspective. Their objective was to investigate scaling effects in small two-stroke ICEs with displacement values smaller than 0.05 dm^3. Due to the exponential increase in the surface-area-to-volume ratio (SA/V_d) as the engine size decreases (given a constant bore-to-stroke ratio), the performance of such engines is predominantly influenced by heat and frictional losses. Consequently, the (SA/V_d) parameter was chosen as a representative indicator of engine size instead of the displacement volume itself. The ratio can be calculated using Equation (10).

$$\frac{SA}{V_d}\ [\text{dm}^{-1}] = \frac{\pi{\cdot}B{\cdot}S + 2{\cdot}\frac{\pi{\cdot}B^2}{4}}{\frac{\pi{\cdot}B^2}{4}{\cdot}S} = \frac{4}{B} + \frac{2}{S} \tag{10}$$

where the bore and stroke are expressed in dm. The authors assumed a constant specific power, ρ_{pwr} (kW/dm^3), and a bore-to-stroke ratio of one. The engine power per cylinder can then be scaled with the displacement volume to give:

$$P_{rated}\left[\frac{\text{kW}}{\text{cyl}}\right] = \rho_{pwr}{\cdot}V_{cyl} = \rho_{pwr}{\cdot}\pi{\cdot}\frac{B^3}{4} \tag{11}$$

where V_{cyl} $\left(\mathrm{dm}^3\right)$ is the displacement volume of a single cylinder. Bringing the surface-area-to-volume ratio inside Equation (11) results in the following scaling law:

$$P_{rated}\left[\frac{\mathrm{kW}}{\mathrm{cyl}}\right] = \frac{\rho_{pwr}\cdot\pi}{4}\cdot\left(\frac{SA/V_d}{6}\right)^{-3} \tag{12}$$

Rowton et al. [42] validated their scaling law across a diverse range of ICEs. This range extended from miniature model engines with a displacement as small as 0.0055 dm^3 to conventional, light-duty engines with 2 dm^3 of displacement. The coefficients defining the curve can be found in Table 1, and they exhibit a strong alignment with the theoretically derived values. Note that a lower accuracy would be obtained when writing the total engine power as function of SA/V_d. This is because the surface-area-to-volume ratio is independent of the number of cylinders $\mathrm{N_c}$. If both sides of Equation (12) were multiplied by N_c, it would result in the total power output being dependent on two variables as opposed to one.

Employing a similar methodology to formulate the scaling law described in Equation (12), Rowton also developed analogous scaling laws with respect to SA/V_d for the brake fuel conversion efficiency, normalized friction power and normalized heat loss in his thesis work [43]. Given our primary focus on performance parameters, only the brake fuel efficiency correlation is shown here:

$$BTE\ [\%] = 664.08\cdot\left({}^{SA}/_{V_d}\cdot 1\ \mathrm{dm}^3\right)^{-1.5} \tag{13}$$

Similarly to Equation (2), the efficiency increases with an increase in the displacement volume and a respective smaller surface-area-to-volume ratio. For engines in the size range from 0.025 dm^3 to 0.1 dm^3, an effort was also made to express Equation (13) solely as a function of the displacement volume:

$$BTE\ [\%] = 395.285\cdot\left(\frac{V_d}{1\ \mathrm{dm}^3}\right)^{1.5} + 7 \tag{14}$$

Extrapolating Equations (13) and (14) beyond their design space, however, leads to meaningless results.

The scaling laws detailed above have been summarized based on their mathematical formulations in Table 1. It is worth noting that certain coefficients may not align with the values found in the respective source references. This discrepancy arises from the objective of standardizing these scaling laws by expressing them all in consistent units, with power denoted in kW and displacement in liters (dm^3). Consequently, the unit of the constant *a* also varies for each scaling law, ensuring the commensurability of units between the left and right sides of the equation.

Since these curve-fitted equations are all written as mathematical functions of the engine size, their biggest advantage is their ease of implementation and rapid response within whole-energy ESOMs. The downside of this approach, however, is that by lumping together all the other operating characteristics (e.g., fuel type, combustion type (SI vs. CI), turbocharger specification, compression ratio, AFR, spark timing, injection timing, etc.) into one volume-specific power constant '*a*' (see mathematical form in Table 1), their individual impact on the performance parameters gets lost, and hence the accuracy of the prediction diminishes. This lack of accuracy is especially true for scaling laws based on Equations (1) and (12), where the only variable is the displacement volume. A level of improvement has been added to those equations which incorporate the engine speed and load (Equations (4), (6), (7) and (9)) into their formula. However, typically, no more than three or four variables are employed in the right-hand side of these equations. Hence, it becomes the responsibility of the end user to maintain a comprehensive understanding of the data set. Optimal results are achieved when engines with similar operating characteristics are employed. Having knowledge of all the specifications also enables users to better account

for any scatter or outliers that may appear when plotting the performance parameters as a function of the engine size only.

Table 1. Performance correlation functions.

Power (kW)					
$y = a \cdot x_1^b \cdot x_2^c$					
Reference	x_1	x_2	a	b	c
Menon et al. [34]	V_d (dm^3)	1	27.654	0.9543	0
Brown et al. [35]	V_d (dm^3)	1	37.349	0.74	0
Chon et al. [39]	V_d (dm^3)	1	49.435	1	0
Chon et al. [39]	A (dm^2)	1	-	-	0
Heywood et al. [41]	V_d (dm^3)	N_c	-	2/3	1/3
Rowton et al. [42]	SA/V_d (dm^{-1})	1	27,583	−3.1	0
Rated Power (kWs/m)					
$y = a \cdot x^b$, $y = P/c_m$					
Reference	x		a	b	
Chon et al. [39]	A (dm^2)		2.6	1	
Torque (Nm)					
$y = a \cdot x$					
Reference	x			a	
Chon et al. [39]	V_d (dm^3)			90.888	
BTE (%)					
$y = a \cdot x^b + c$					
Reference	x	a	b	c	
Menon et al. [34]	V_d (dm^3)	24.644	0.0688	0	
Rowton et al. [43]	SA/V_d (dm^{-1})	664.078	−1.5	0	
Rowton et al. [43]	V_d (dm^3)	395.285	1.5	7	

Another significant consequence of these curve-fitted equations is that there are no inherent limitations on the operating envelope. The displacement volume can be increased or decreased without ever running into the thermodynamic limits of an ICE. Especially for SI engines, the maximum bore size is eventually restricted by knock phenomena. Additionally, as the bore size increases, combustion can become unstable due to the finite flame speed. Such changes can impact both the efficiency and specific power; however, these effects are not currently accounted for in these models.

2.2. Available Engine Data

As pointed out in the previous paragraph, the predictive capabilities of these scaling laws are heavily contingent on the availability of engine performance data that can be used for curve-fitting. A reliable fit and thus accurate predictions can only be obtained when examining engines using the same type of fuel technology. This presents a particular challenge for renewable synthetic fuels. Since they are best suited for SI operation, heavy-duty performance data are relatively scarce. An increase in bore size is typically linked with a reduction in engine speed, which can elevate the risk of abnormal combustion phenomena like knocking. However, an increased bore diameter also extends the flame travel time, leading to a more even distribution of heat release and a reduction in the unburned mixture pressure and temperature [44]. Moreover, renewable fuels like hydrogen, methane and light

alcohols such as methanol and ethanol possess significantly higher laminar flame speeds compared to conventional gasoline. As a result, they consume end gases more rapidly. Especially for liquid methanol and ethanol, where the strong evaporative cooling further reduces the tendency for knocking, these fuels have the potential to enable high-efficiency and high-power performance akin to their diesel competitors.

In Table 2, a summary of the collected data is presented, focusing on large-bore spark-ignited engines running on alternative fuels. The engines are categorized into three different technology groups: stoichiometric engines, lean-burn open-combustion-chamber engines and lean-burn pre-chamber engines. The selection of engines in this table begins with a bore diameter equal to or exceeding 95 mm, a boundary considered as the upper limit for automotive-sized engines [40].

Notably, only three OEMs have recently published information on their hydrogen spark-ignition prototype engines [45–48]. Furthermore, following a collaboration, both Deutz AG [45] and Keyou GmbH [48] employed the same engine geometry, resulting in only two distinct engine types. For pure methanol operation, only seventeen references and even fewer engines were found in the literature, all summarized in Table 2. There are three engines that operate at stoichiometric conditions and nine that employ lean operation (one with a pre-chamber instead of the conventional open chamber). This insufficiency of data impedes the development of precise map-based models. The same holds true for ethanol-fueled engines, with only two references for pure ethanol use in large-bore spark-ignited engines, namely the works of Mahendar et al. [49] and Li et al. [50]. However, E85, a fuel blend with 85 vol% ethanol and 15 vol% gasoline, has been studied to a slightly greater extent, with three references exploring stoichiometric operating conditions [51–53].

Table 2. Overview of SI test engines running on hydrogen, methanol and ethanol.

Hydrogen					
Reference	**B (mm)**	**V_d (dm^3)**	**N_c (-)**	**Stoichiometric Operation? (Yes/No)**	**Pre-Chamber? (Yes/No)**
Koch et al. [47,48]	110	7.8	6	No	No
Nork et al. [45]	110	7.8	6	No	No
Sommermann et al. [46]	145	16.8	6	No	No
Methanol					
Zhen et al. [54–58]	100	3.99	4	Yes	No
Li et al. [50]	100	3.99	4	No	No
Zhu et al. [59]	123	10.3	6	No	No
Mahendar et al. [49]	127	1.95	1	Yes	No
Mahendar et al. [49]	127	1.95	1	No	No
Gong et al. [60,61]	130	2	1	No	No
Björnestrand et al. [62]	130	2.12	1	No	No
Li et al. [63]	130	2.12	1	No	No
Güdden et al. [64]	-	2.13	1	Yes	No
Bosklopper et al. [65]	170	34.5	8	No	No
Güdden et al. [64]	-	5	1	No	No
Leng et al. [66]	320	33.78	1	No	Yes

Table 2. *Cont.*

Hydrogen					
Reference	**B (mm)**	**V_d (dm^3)**	**N_c (-)**	**Stoichiometric Operation? (Yes/No)**	**Pre-Chamber? (Yes/No)**
Ethanol (E100)					
Li et al. [50]	100	3.99	4	No	No
Mahendar et al. [49]	127	1.95	1	Yes	No
Mahendar et al. [49]	127	1.95	1	No	No
Ethanol (E85)					
Brusstar et al. [51]	95	4.5	6	Yes	No
Kumar et al. [52]	104	5.76	6	Yes	No
Ottosson and Zioris [53]	127	1.95	1	Yes	No

When considering methane as a fuel, the landscape differs significantly. The cost-effectiveness and abundancy of natural gas [67,68], along with its lower environmental impact compared to gasoline and diesel, has increased the share of gas-fueled heavy-duty engines over the years. By 2019, natural gas spark-ignition engines accounted for 14.4% of reciprocating engine power generation orders [69]. Based on their air-to-fuel ratio, they can be divided into two major groups, the stoichiometric and the lean-burn types. Stoichiometric engines can effectively employ a three-way catalyst (TWC) aftertreatment system, enabling ultra-low tailpipe emissions of NO_x, CO and THC, while remaining significantly more cost-effective compared to conventional diesel aftertreatment systems [70–72]. However, they are limited in their ability to achieve high BMEP values due to high thermal stresses and knocking propensity at elevated in-cylinder temperature conditions. For example, the MAN E2842, a 21.9 dm^3, 12-cylinder SI NG engine with a bore diameter of 128 mm can reach up to a 9.13 bar BMEP under stoichiometric conditions [73]. Through the utilization of a Miller cycle to reduce the effective compression ratio and a redesigned turbocharger to handle the high exhaust temperatures, the Waukesha VHP Series Five SI gas engine, featuring a bore size of 238 mm, can reach even higher levels up to 12.29 bar BMEP [74]. One approach to enhancing the performance is by reducing in-cylinder temperatures using EGR dilution. For instance, Wheeler et al. [75] achieved an engine load of 25 bar IMEP in a medium-duty engine with a 106.5 mm bore by adding 20% EGR, while Zhang et al. [76] demonstrated a 22.18 bar BMEP in a 11.9 dm^3, six-cylinder heavy-duty truck engine with a bore diameter of 130 mm, employing 17.8% EGR. The lower combustion temperatures achieved with EGR also enhance the thermal efficiency by reducing heat and endothermic dissociation losses [77,78] while reducing the risk of knocking. This allows for a higher and advanced spark timing that is closer to the minimum advance for best torque (MBT) timing.

Another approach to reduce in-cylinder temperatures is by introducing an excess of air into the combustion chamber, which, similar to EGR operation, promotes lean combustion. Lean combustion can enhance the brake thermal efficiency by reducing heat losses, endothermic losses and the likelihood of knocking [79,80]. However, applying these principles to large-bore SI engines with natural gas is challenging. The slower burning velocity of methane limits its lean-burn capabilities [81], which can lead to incomplete combustion and misfires. Nevertheless, Wu et al. [82] demonstrated the feasibility of lean combustion in a 190 mm bore engine with a compression ratio of 10:1 by optimizing the combustion chamber shape to generate the appropriate turbulence intensity for complete combustion.

To achieve even higher performance, modern gas engines utilize a pre-chamber design. This design incorporates a second combustion chamber with volumes of less than 3% of the clearance volume of the main chamber, integrated into the spark plug design [83]. The pre-

chamber is less affected by charge motion in the main chamber, providing more favorable conditions for igniting a lean mixture. After ignition, the pressure rise generates strong flame jets that flow out of the pre-chamber, offering two key advantages [84]. Firstly, a distributed ignition source is created in the main chamber, resulting in shorter combustion durations, compensating for the lower burning velocity of natural gas. Secondly, the flame jets consist of complete and partial combustion products with active species, further enhancing the ignition of the charge. This design has enabled the development of a wide range of SI engines, ranging from a 131 mm bore engine [85] to the world's largest-bore gas engine with a diameter of 560 mm [86]. State-of-the-art engines at the high end of the scale include the Jenbacher J920 engine, a 20-cylinder, 310 mm bore engine with a thermal efficiency of 51% at an engine load of 24 bar BMEP. This engine delivers 10.4 MW of electrical power at an operating speed of 1000 rpm [87]. Similarly, the 20-cylinder MAN V35/44G engine with two-stage turbocharging and a bore size of 350 mm achieves a 24.2 bar BMEP with an efficiency of 51%, resulting in an output power of 12.8 MW at an operating speed of 750 rpm [88]. Lastly, the MAN V51/60G features two-stage supercharging and 18 cylinders with a bore size of 510 mm. When optimized for the specific power output, the engine delivers 20.7 MW (22.5 bar BMEP) with an efficiency of 50%, while optimization for efficiency results in 18.9 MW (20.56 bar BMEP) at an efficiency of 52% [89].

There are a substantial amount of engine data available for SI gas engines with a pre-chamber, which provides a sufficient basis for assessing the performance of the curve-fitted scaling laws. The next section applies these scaling laws to a data set consisting of 28 engines. The results can be used to predict the performance parameters of similar but differently sized engines.

2.3. Curve-Fitted Equations for Large-Bore SI NG Engines with Pre-Chamber Combustion

To conclude this part, a case study was conducted on a set of heavy-duty SI gas engines equipped with a pre-chamber spark plug and operating under lean conditions. The data set comprises 28 engines, with data drawn from both the scientific literature [67,85,86,90–104] and documentation from commercial OEMs [87–89,105–108]. Figure 1 depicts the only scaling law for torque versus the displacement volume. As expected from Equation (3), the relationship is nearly perfectly linear. The mean rated BMEP corresponds to 4π times the slope of the regression curve, resulting in 21.33 bar for the large, four-stroke pre-chamber gas engines included in this study. This value serves as a benchmark for engine manufacturers to remain competitive in today's engine market and represents the current state of the art within this particular engine class. With an R^2 value of 0.9971, the accuracy of the scaling law across such a wide range of displacement volumes is noteworthy.

Figure 2 shows the relationship between the rated power (kW) and the total cylinder volume (dm^3). According to Equation (4), a linear relationship was initially assumed between the engine output and engine size. However, a significant deviation from this trend became evident, particularly for engines with bore diameters exceeding 500 mm. The decline in the specific power (kW/dm^3) was primarily attributed to the lower operating speed of these large engines. While the relatively smaller engines operate at engine speeds of 750 rpm and beyond, the three engines represented by orange dots operate at 500 rpm, and the one depicted by the green diamond operates at a mere 375 revolutions per minute. To achieve a more accurate fit, the equation associated with the linear scaling law omits these four data points. Due to their lean combustion operation, these large-bore SI gas engines struggle to attain a specific power level exceeding 13.91 kW/dm^3, highlighting the challenges posed by abnormal combustion behavior in such engines. By way of comparison, light-duty naturally aspirated SI engines typically exhibit specific power values ranging from 40 to 65 kW/dm^3, with turbocharged SI engines reaching levels as high as 80 kW/dm^3 [40].

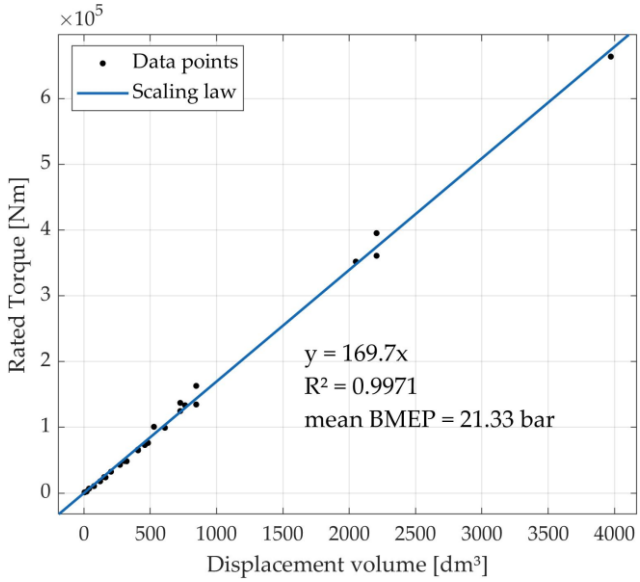

Figure 1. Curve-fitted equations of rated torque (Nm) versus displacement volume (dm^3).

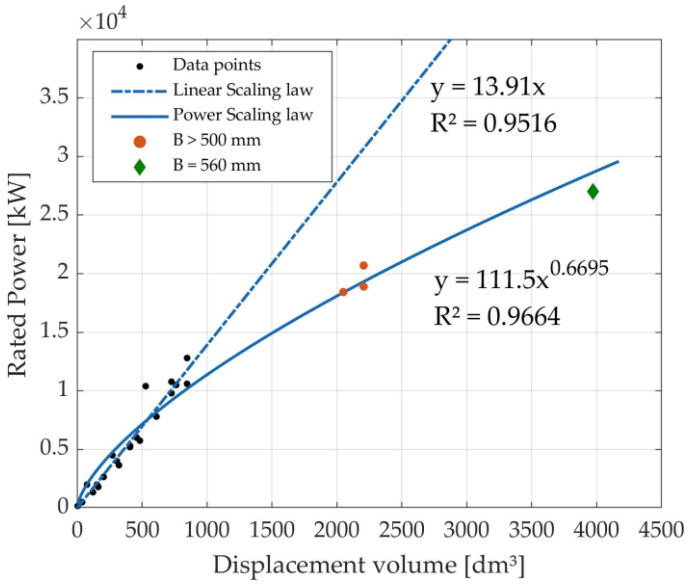

Figure 2. Both linear and power trendlines for rated power (kW) versus displacement volume (dm^3). The linear trend line is correlated only to engines with a bore size smaller than 500 mm.

A power trend line partly covers up the issue of lower engine speeds. By applying Equation (1), the coefficient of determination can be increased from 0.9516 to 0.9664. A more effective approach is to rewrite the engine speed as function of the mean piston speed c_m (m/s) (Equation (5)). The resistance to gas flow into the cylinder imposes an upper limit on c_m of around 15 m/s, irrespective of the engine size [40]. Additionally, especially for large-bore engines, inertia forces further restrict the piston's achievable speed. Although Figure 3 demonstrates some scatter in the data set related to the mean piston speed, utilizing scaling law (6) increases the R^2 value to 0.9813. The most accurate fit is achieved by normalizing the rated power with the mean piston speed. In this case, the slope of the curve becomes solely a function of the BMEP at the rated power, as indicated by Equation (7). As previously discussed, the BMEP is considerably less affected by the engine size, given its role as a vital performance parameter that must meet market demands.

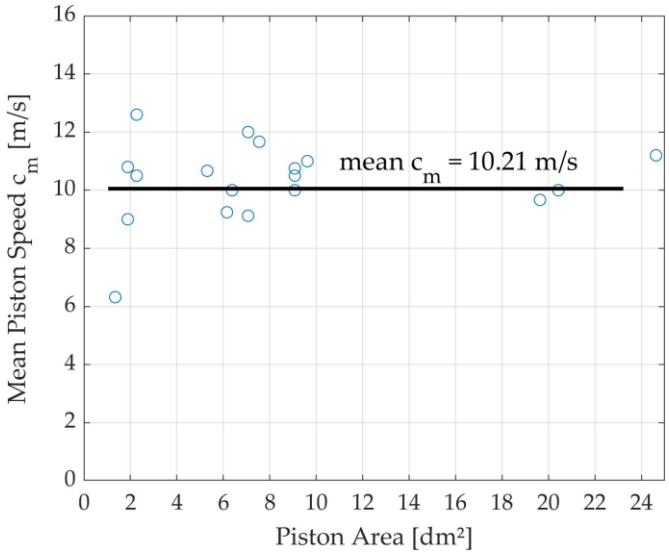

Figure 3. Mean piston speed (m/s) as a function of piston area per cylinder (dm^2). The horizontal black line shows the mean value of the data set.

Figure 4 presents the scaling law for normalized power (kWs/m) plotted against the total piston area (dm^2) scaling law. For a given mean piston speed value, this scaling law offers the most accurate prediction of power for a specific engine size, achieving a high R^2 value of 0.9935. Equations (9) and (12) were also examined but yielded less-favorable results, as reflected in the R^2 values. The details of these equations, including their respective scaling laws and the coefficients of determination, are shown in Appendix A. In Equation (9), the parameter c_m remains a factor, resulting in a similar predictive behavior as Equation (6). On the other hand, Equation (12), derived from the work of Rowton et al. [42], assumes a constant specific power (kW/dm^3). However, as observed in Figure 2, the specific power varies significantly for engines with bore sizes exceeding 500 mm. Furthermore, the correlation in Equation (12) is based on the surface-area-to-volume ratio, a critical factor in small engines. In the case of large-bore engines, with SA/V_d being inversely related to the engine size (Equation (10)), this factor has a relatively minor impact and undergoes only marginal changes across the range of engines investigated. Nevertheless, both equations exhibit a strong power-law dependence on engine size, with R^2 values of 0.9805 and 0.9671, respectively.

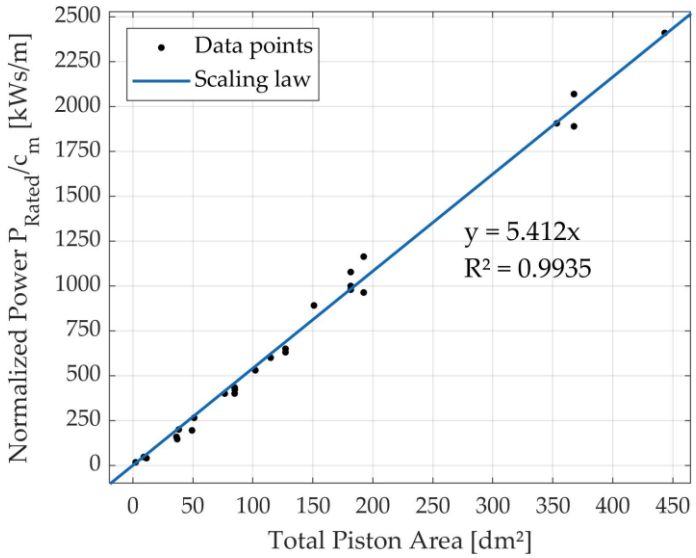

Figure 4. Normalized rated power (kWs/m) as a function of total piston area (dm^2).

Finally, three laws were introduced to scale the brake thermal efficiency. Given that the BTE is already a dimensionless parameter, its dependence on engine size was anticipated to be relatively low. Figure 5 shows the correlation that best aligns with the data. Since there is no derivation of Equation (14) provided in reference [43], the data were fitted to a similar curve with the form $y = ax^b + c$. A slight increase in efficiency is seen for the larger engines, primarily because of their marginally reduced surface-area-to-volume ratio, resulting in lower heat and friction losses. The combustion efficiency on the other hand is lower for these large engines due to the challenges associated with maintaining stable combustion throughout the entire combustion chamber.

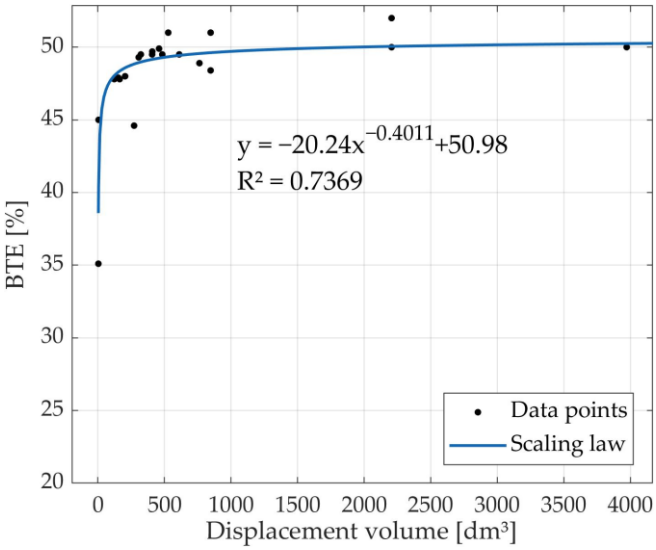

Figure 5. BTE (%) as a function of displacement volume (dm^3). The correlation is based on Equation (14).

A summary of the accuracy of fit for all the scaling laws tested is provided in Table 3. Rated power scales most effectively with the total piston area, as described by Equation (6). Increasing the total piston area A_p can be achieved by either increasing the number of cylinders in the engine or by enlarging the bore size of each cylinder, as detailed in Equation (8). On the other hand, the brake thermal efficiency is best predicted using a scaling law based on Equation (14). However, when examining the R^2 values for BTE scaling, it becomes apparent that only a portion of the variation in efficiency can be attributed to the engine size. The substantial scatter observed in the efficiency data was attributed to other operational characteristics, as discussed earlier, such as valve timing, compression ratio, spark timing, etc.

Table 3. Estimation of fit based on R^2 values. The best performing scaling laws are set in bold.

Torque (Nm)		**Rated Power (kWs/m)**	
Scaling law	R^2	Scaling law	R^2
Equation(3)	**0.9971**	**Equation (7)**	**0.9935**
Power (kW)		**BTE (%)**	
Scaling law	R^2	Scaling law	R^2
Equation (1)	0.9664	Equation (2)	0.6495
Equation (4)	0.9516	Equation (13)	0.5168
Equation(6)	**0.9813**	**Equation(14)**	**0.7369**
Equation (9)	0.9805		
Equation (12)	0.9671		

Due to the inherent dependency of these types of scaling laws on the input data (experimental and validated numerical engine data on synthetic e-fuels) and the current absence of them, alternative approaches were also investigated where no such test data were needed. They are explained and discussed in the next sections.

3. Alternative Methods

3.1. Willans Line Method

The Willans line method can be used to scale and predict the brake thermal efficiency and fuel consumption map of an internal combustion engine based on the knowledge of one reference engine of the same class. The original Willans line representation is very generic and simply assumes that for an ICE at a constant engine speed, an affine relationship between the input power and output power exists [109]. In other words, at a constant speed, the relationship between the load and fuel consumption is linear. Figure 6 provides a visual representation of this model, which can be mathematically expressed using Equation (15):

$$P_{out}\ [\text{kW}] = e \cdot P_{in} - P_{loss} \tag{15}$$

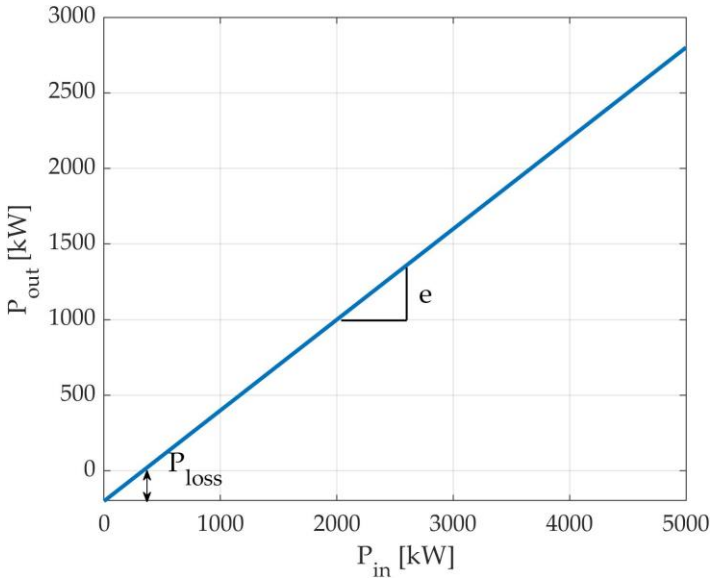

Figure 6. The linear relationship between input power (kW) and output power (kW) at a constant engine speed.

Parameter 'e' denotes the net indicated thermal efficiency, while P_{loss} accounts for external energy losses, encompassing mechanical friction losses and losses attributed to auxiliary components. Rizzoni et al. [110] extended this formulation to make it independent of the power rating or displacement volume, making it convenient for engine scaling. Since the speed is assumed to be constant, Equation (15) can be reformulated as follows:

$$T_{out}\ [\text{Nm}] = e \cdot \frac{\dot{m}_f H_u}{\Omega} - T_{loss} \tag{16}$$

where $\dot{m}_f$ and H_u are the mass flow rate (kg/s) and the lower heating value (MJ/kg) of the fuel, respectively, and Ω is the angular speed (rad/s). In Equation (16), both the torque and angular speed remain dependent on the engine size. This dependency can be addressed by incorporating the concept of mean effective pressures. The mean effective pressure normalizes the torque over an engine cycle with the total displacement volume:

$$BMEP\ [\text{Pa}] = \frac{4\pi \cdot T_{out}}{V_d} \tag{17}$$

$$AMEP\ [\text{Pa}] = \frac{4\pi}{V_d} \cdot \frac{\dot{m}_f H_u}{\Omega} \tag{18}$$

$$p_{m_{loss}}\ [\text{Pa}] = \frac{4\pi \cdot T_{loss}}{V_d} \tag{19}$$

where *BMEP* represents the brake mean effective pressure, *AMEP* stands for the available mean effective pressure, which signifies the maximum *MEP* achievable if the engine operates at 100% efficiency, and $p_{m_{loss}}$ symbolizes the normalized torque incorporating frictional losses. This reformulation aligns Equation (16) with the dimensionless Willans line method:

$$BMEP\ [\text{Pa}] = e \cdot AMEP - p_{m_{loss}} \tag{20}$$

The engine efficiency can is defined as:

$$\eta\ [-] = \frac{BMEP}{AMEP} \tag{21}$$

Both the indicated thermal efficiency e and the loss factor $p_{m_{loss}}$ are functions of the engine speed. As proposed by Rizzoni et al. [110] these factors can be approximated by low-order polynomial functions of the mean piston speed c_m, which, as previously discussed, is much less affected by the engine size than the engine speed. They put forward the following parametrization:

$$e(c_m) = e_0(c_m) - e_1(c_m) \cdot AMEP \tag{22}$$

$$e_0(c_m) = e_{00} + e_{01} \cdot c_m + e_{02} \cdot c_m^2 \tag{23}$$

$$e_1(c_m) = e_{10} + e_{11} \cdot c_m \tag{24}$$

$$p_{m_{loss}}(c_m) = p_{m_{loss,0}} + p_{m_{loss},2} \cdot c_m \tag{25}$$

It is evident from Equation (22) that the dimensionless Willans line method is no longer an affine function. Nevertheless, introducing nonlinearity into AMEP is sometimes necessary to enhance predictions under high-load conditions.

If now, for one optimized reference engine, the fuel consumption as a function of load is known, the seven efficiency-related parameters in Equations (23)–(25) can be found by curve-fitting the data to Equation (20) using a method such as least-squares fitting. Given that the functions from which they originate are dimensionless, these seven parameters are believed to accurately represent an engine of a specific class, irrespective of its size.

For a new engine within the same engine class, with displacement volume $V_{d,scaled}$ and the same bore-to-stroke ratio *bs* [111], the fuel consumption map for a given torque demand T_{req} can now be computed by following these steps [112]:

$$S_{scaled}\ [\text{m}] = \left(\frac{V_{d,scaled}}{\pi \cdot bs^2} \right)^{\frac{1}{3}} \tag{26}$$

$$c_{m,scaled}\ [\text{m/s}] = 2 \cdot S_{scaled} \cdot N \tag{27}$$

$$BMEP_{scaled}\ [\text{Pa}] = \frac{4\pi \cdot T_{req}}{V_{d,scaled}} \tag{28}$$

$$AMEP_{scaled} = \frac{e_0 - \sqrt{e_0^2 - 4 \cdot e_1 \cdot \left(BMEP_{scaled} + p_{m_{loss}} \right)}}{2 \cdot e_1} \tag{29}$$

Once the efficiency parameters e_0, e_1 and $p_{m_{loss}}$ are determined with the new $c_{m,scaled}$, Equation (18) can be employed to calculate the fuel flow rate of the scaled engine $\dot{m}_{f,scaled}$. The engine's efficiency can be found by substituting these values into Equation (21).

This method primarily finds application in optimizing the size of an ICE in hybrid electric vehicles [111–114]. There is a significant demand for the rapid modeling and computation of fuel consumption maps for engines of varying sizes in this context. However, when it comes to precisely predicting the brake thermal efficiency for a given engine size, this method may not be entirely suitable. Unlike the right-sizing approach for hybrid electric vehicles, the range of displacement volumes that need to be considered in this study is much larger. The curve-fitted equations were employed to examine engines with displacements ranging from 2.1 dm^3 to 4000 dm^3. In such cases, the variation in the surface-area-to-volume ratio becomes important and influences the efficiency by reducing friction forces and heat losses. The engine efficiency, calculated in Equation (21) as the ratio of two dimensionless parameters, remains unaffected by the engine size. Additionally, the power output is not predicted but rather imposed. It is worth noting that the assumption of a constant engine speed can cause problems when dealing with significant differences in the displacement volume between the scaled engine and the reference engine. Since the mean piston speed is limited, the engine displacement can only be increased until the maximum value of c_m is reached. Finally, a problem that this method has in common with the curve-fitted equations is that both methods fail to implement boundary conditions or constraints. It is essential to define an upper limit beyond which these methods remain valid.

In conclusion, the complexity of the prediction method needs to be increased in order to provide a more accurate framework to scale internal combustion engines. However, the advantage of needing only one reference engine is a key feature that should be retained when exploring alternative scaling methods.

3.2. Similitude

A more detailed approach than the one used by the Willans line method can be accomplished through similitude analysis. Under a set of initial and boundary conditions, the results of one reference design can be scaled up or down to attain the same dimensionless performance parameters as the reference design for any arbitrary design. The concept is rooted in the idea that physics is inherently dimensionless [115] and has been employed in various engineering fields, including structural engineering, fluid mechanics, vibration and impact problems [116]. In the context of internal combustion engines, it would mean that if two engines would reach similitude, their dimensionless performance parameters BTE (%), specific power (kW/dm^3) and specific emissions (g/kW) would be identical.

For example, consider the 33.78 dm^3, single-cylinder pre-chamber methanol-fueled SI engine investigated by Leng et al. [66] (Table 2). This engine achieved an indicated thermal efficiency of 48.1% at a rated power of 439 kW. When using this engine as the reference engine, achieving similitude implies that the ITE remains constant at a value of 48.1% across all different engine platforms, and the power output follows the scaling law expressed in Equation (30):

$$P_{rated}\ [\text{kW}] = 13 \cdot \left(\frac{\text{kW}}{\text{dm}^3} \right) \cdot V_d \tag{30}$$

where the displacement volume is in dm^3. Note here that for the investigated methanol engine, the specific power (13 kW/dm^3) is consistent with the values found for NG engines (as shown in Figure 2). This indicates the potential of methanol as an alternative fuel in large-bore SI engines. The scaling law proposed based on the similitude analysis shares the same form as the one proposed by Chon et al. [39].

Given that the heavy-duty industry has traditionally been dominated by compression-ignition engines, the search for the initial and boundary conditions under which similitude can be achieved has primarily focused on conventional diesel combustion (CDC) mode. The theoretical foundation for describing diesel combustion processes with dimensionless parameters began as early as 1906 with the work of Lanchester et al. [117]. However, it

was not until 1988 that Chikahisa et al. [118] theoretically demonstrated the possibility of achieving similarity in diesel compression-ignition engines. This analysis relied on two important assumptions: first, they assumed that the fuel spray could be treated as a gas jet due to the small size of the droplets, which evaporate almost instantly under very high pressures. Second, combustion was assumed to take place diffusively, with the reaction rate controlled by the mixing of fuel and air. Based on these assumptions, Chikahisa et al. identified the following requirements for achieving similitude [118]:

1. The combustion chamber and injection system must be geometrically scaled.
2. The fuel should have the same stochiometric air-to-fuel ratio and the same nondimensional heating value H_u/c_pT_0.
3. The fuel mass flow rate for each crank angle $\dot{m}_f(\theta)$ should be proportional to the density times the third power of the bore, $\rho_0 B^3$.
4. The swirl ratio must be equal.
5. The ratio $(N \cdot B)/(60 \cdot u_0)$ must be equal for both engines.
6. The fuel droplet diameter should be made proportional to $\sqrt{B/u_0}$ by controlling the injection pressure, fuel viscosity and surface tension of the fuel.
7. The cylinder wall temperature must be controlled to give the same heat transfer effect.
8. The ignition delay must be equal in crank angle degree.

For the above, H_u is the lower heating value of the fuel (J/kg), and c_p, T_0 and ρ_0 are the fuel's heat capacity at constant pressure (J/K), temperature (K) and density (kg/m^3), respectively. u_0 is the injection rate of the fuel (m/s), and N is the engine speed.

The assumptions outlined above also imply the need for equal ambient conditions. The ratio of the cylinder charge density and fuel density, which is dependent on the applied boost pressure, should be consistent. Requirement (5) is derived from the fact that the working volume of the large and small engine need to change proportionally during the engine cycle [119]. Considering the degrees of freedom in Requirement (5), Chikahisa et al. [120] suggested maintaining a constant engine speed N for engines of different sizes. However, keeping the engine speed constant imposes limitations on the scaling range, similar to the Willans line method. As the engine size increases with a constant engine speed, the mean piston speed c_m will be the limiting factor for large-bore engines. Bergin et al. [121] took a different approach and recommended keeping the fuel injection pressure constant between the two engines. According to Bernoulli's principle, this implies that the ratio of the injection rates must also remain constant:

$$\Delta p = \frac{1}{2} \cdot \rho_0 \cdot u_0^2 \tag{31}$$

Combining Equation (31) and Requirement (5) shows that engine speed should be inversely scaled with the ratio of the bore diameters of both engines r, while the mean piston speed remains constant under constant injection pressures:

$$\frac{N_{scaled}}{N_{ref}} = \frac{B_{ref}}{B_{scaled}} = \frac{1}{r} \tag{32}$$

Stager and Reitz [122] extended the work of Bergin et al. [121] by adding a constraint on the lift-off length H. The flame lift-off length is defined here as the distance away from the injector nozzle's exit where the flame stabilizes during the quasi-steady phase of the spray's development [40]. This lift-off length can be calculated using an empirical power-law relationship presented by Pickett et al. [123]:

$$H\,[m] \propto d_o^{0.34} \cdot u_0 \tag{33}$$

where d_0 is the injector nozzle orifice diameter (m). In order to achieve similitude, the flame lift-off length should scale with the ratio of the bore diameters as follows:

$$\frac{H_{scaled}}{H_{ref}} = r \tag{34}$$

By combining both Equations (33) and (34), the new relationship for the injection rate of fuels can be found. From there, Equation (31) can be used to calculate the relationship for the injection pressures and Requirement (5) for the engine speeds.

In 2018, Zhou et al. [119] labeled the three different approaches above as the speed rule (S-law), the pressure rule (P-law) and the lift-off rule (L-law), respectively, depending on which factor they keep constant. More importantly, they revised the theoretical derivation made by Chikahisa et al. [118]. Firstly, they reevaluated the assumption that the fuel spray could be treated as a gas jet and demonstrated that evaporating sprays could reach similitude similar to jet flow. However, this is only possible when the spray cone angle α of the diesel injection is equal for both engines. Given that both the S-law and the L-law change the injection pressure between the scaled engine and the reference engine, the spray angle will vary as well, making it challenging to achieve similitude. In contrast, the P-law keeps the injection pressure constant and is more favorable for achieving spray similitude. Secondly, Zhou et al. proved that diesel similarity can also be reached under premixed combustion conditions. In this case, the reaction rate is controlled both by the mixing rates and chemical reaction rates, subject to the condition of Equation (35):

$$\frac{B_{scaled}}{u_{0,scaled}} = \frac{B_{ref}}{u_{0,ref}} \tag{35}$$

Substituting Equation (35) into Requirement (5) reveals that adhering to the conditions of the S-law is necessary to achieve similitude in premixed diesel combustion conditions. Table 4 provides a summary of the requirements needed, based on the theoretical derivation, to maintain constant dimensionless performance parameters for all three different approaches (S-law, P-law and L-law).

Table 4. Initial and boundary conditions to reach similitude for the three proposed methods [119].

Conditions to Meet	S-Law	P-Law	L-Law
Geometric similarity			
Dimensions ($\frac{B_{scaled}}{B_{ref}}$, $\frac{S_{scaled}}{S_{ref}}$, $\frac{d_{0,scaled}}{d_{0,ref}}$)	r	r	r
Kinematic similarity			
Ratio of swirl ratios $\left(SR_{scaled}/SR_{ref}\right)$	1	1	1
Injection rate ratio $\left(u_{0,scaled}/u_{0,ref}\right)$	r	1	$r^{2/3}$
Engine speed ratio $\left(N_{scaled}/N_{ref}\right)$	1	r^{-1}	$r^{-1/3}$
Others			
Fuel mass flow rate ratio $\left(\dot{m}_{f,scaled}/\dot{m}_{f,ref}\right)$	r^3	r^3	r^3
Injection duration ratio $\left(\tau_{scaled}/\tau_{ref}\right)$ (s)	1	r	$r^{1/3}$
Injection pressure ratio ($\Delta P_{scaled}/\Delta P_{ref}$)	r^2	1	$r^{4/3}$

In practice, despite adhering to these requirements, achieving perfect similarity is not always possible. The degree of similarity may vary depending on the load tested, the chosen scaling rule and the specific performance parameter of interest. Researchers have observed that different scaling rules are preferable for different aspects of engine performance.

Zhou et al. [124] stated that the P-law is more preferable for scaling in-cylinder pressures and temperatures and the indicated thermal efficiency, while the S-law may better predict the premixed combustion processes and pollutant emissions. Other researchers, like Shi et al. [125], found that the L-law might not scale the heat release rate (HRR) and exhaust emissions as effectively under medium-load conditions compared to low-load conditions.

Staples et al. [126], on the other hand, conducted experiments to investigate the P-law and the L-law. They found that both laws could scale the combustion parameters well under medium-load conditions, including the indicated mean effective pressure (IMEP), indicated specific fuel consumption (ISFC), in-cylinder temperatures and pressures and combustion phasing. However, emissions did not scale well, mainly due to the difference in engine speed under both laws (see Table 4) and the difference in heat transfer losses.

The disagreement in terms of heat transfer losses between the scaled engine and the reference engine is an inherent issue of the similitude approach and is present for all three scaling rules. As the engine displacement volume increases, the surface-area-to-volume ratio decreases, deteriorating the scaling of the important performance parameters. Both heat loss and friction loss decrease, resulting in increased efficiency and power output.

To mitigate these issues, researchers have proposed practical implementations to ensure the original intent of achieving identical dimensionless results. Methods to address the difference in heat transfer between the large and the small engines include increasing the temperature of the intake gases [127–130] or cylinder walls [120,121,126,131] of the smaller engine.

It could be reasoned, however, that aiming for the same results in differently sized engines is not the ideal approach. With a smaller SA/V_d ratio, one should strive for a larger brake thermal efficiency instead of adapting the engine to reach the BTE of the smaller engine. Researchers, such as Zhou et al. [124], have developed scaling laws, similar to the curve-fitted equations, that account for the observed differences between the reference engine and the scaled engines as a function of the bore diameter ratio r.

For the indicated thermal efficiency, Zhou et al. found that instead of achieving identical values, the efficiency values changed according to the functions shown in Figure 7. As expected, all three functions confirm that the efficiency increases with the bore diameter, owing to the reduced heat transfer loss. Analyzing the exponent α of each function $y = x^{\alpha}$ allows for an estimation of how much the outcome of each scaling rule deviates from similitude. In this context, the offset of the ITE is the highest when adhering to the boundary conditions postulated by the S-law, as indicated by the values of α (0.036 > 0.027 > 0.011).

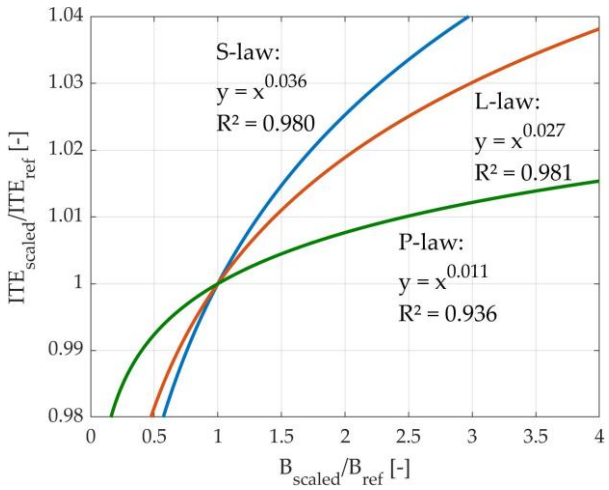

Figure 7. Power functions correlating the difference in indicated thermal efficiency as a function of the ratio of bore diameters r. For each scaling rule, both the mathematical expression as well as the R^2 value have been given [124].

The power functions can be reformulated in terms of the displacement volume to present equations similar to those in Table 1. Assuming a constant bore-to-stroke ratio, the ratio of the displacement volumes becomes one third of the bore ratio:

$$\left(\frac{B_{scaled}}{B_{ref}}\right) = \left(\frac{V_{d,scaled}}{V_{d,ref}}\right)^{\frac{1}{3}} \tag{36}$$

For the P-law at high load, expressing the indicated thermal efficiency (%) as a function of the displacement volume yields, for example, Equation (37):

$$ITE_{scaled}\ [\%] = 50.63 \cdot V_{d,scaled}^{0.004} \tag{37}$$

These types of scaling laws, combined with the scaling rules outlined in Table 4, provide a strong starting point for evaluating the performance of a differently scaled engine based on the characteristics of one optimized reference engine. The latter allows for reducing the number of design parameters when developing new engine models, while the former allows for a good prediction of the performance values.

However, it is important to note that while considerable work has gone into developing the scaling rules for conventional diesel combustion, relatively little research has been conducted on other combustion modes. Shi et al. [131] numerically explored two engines under homogeneous-charge compression-ignition (HCCI) conditions in order to investigate the scaling performance of the L-law in the absence of spray mixing and charge preparation. Their findings indicated that the lift-off rule works effectively for scaling engines operating under HCCI conditions, suggesting that it accounts for the influence of chemistry timescales on the combustion and emissions. However, Lee et al. [127] confirmed that the lift-off rule was inadequate for properly scaling low-temperature-combustion (LTC) conditions due to the lack of importance of the lift-off length in premixed combustion systems. They recommended using the speed rule (S-law) to maintain an identical timescale for chemical reactions. This proposal, though, was questioned by Chuahy et al. [130] while developing scaling rules for reactivity-controlled compression-ignition (RCCI) combustion. While it is possible to adequately scale combustion phasing by keeping the engine speed constant, they pointed out that the BTE would still vary due to changes in heat transfer friction losses, which are function of the mean piston speed.

Therefore, they introduced a new scaling rule applicable to highly premixed, kinetically controlled combustion systems. Using a zero-dimensional, single-zone analysis, they found that the most effective way to maintain constant BTEs was to scale the engine speed with the bore size:

$$\frac{N_{scaled}}{N_{ref}} = \frac{B_{ref}}{B_{scaled}} = \frac{1}{r} \tag{38}$$

Although starting from a different perspective, this leads to similar requirements as dictated by the pressure rule (Table 4).

For spark-ignited operation, unfortunately no scaling rules have been developed so far. The authors presume that this is firstly due to a former lack of interest in large-bore spark-ignition engines. For standard gasoline, the increase in the bore size is limited due to the risk of abnormal combustion phenomena such as knocking. Nonetheless, current research has shown that with fast-burning alternative fuels, bore diameters in the same range as those in heavy-duty diesel engines can be achieved. As a result, engine developers could greatly benefit from the development of such scaling rules. Still, finding a way to deal with the constraints of SI engines will prove to be more challenging than it is for conventional diesel combustion. In CDC operation, the boundaries of scaling the reference engine are limited by the maximum value of the mean piston speed, fuel injection pressure and engine speed [124]. For SI operation, the biggest problem will be to assess knocking combustion. A first idea can be to make use of the Livengood and Wu autoignition integral,

an empirical model designed to predict the autoignition of unburned mixtures in spark-ignition engines [132]:

$$\int_{t_{IVC}}^{t_{KO}} \frac{dt}{\tau(t)} = 1 \tag{39}$$

where t_{IVC} and t_{KO} are the time at the intake valve closing and knock onset, respectively. $\tau(t)$ is the instantaneous autoignition delay time. When the knock integral reaches a value of one, auto-ignition has occurred. With an increase in the bore size, the engine speed generally decreases to keep the mean piston speed limited. A lower engine speed increases the timestep dt (s/°ca), which will increase the chances of the integral reaching one. The latter can be used as a constraint on the increase in the bore diameter when scaling.

4. Summary and Conclusions

In the pursuit of more accurate simulations of future energy systems, this review paper provides a concise summary of scaling laws found in the literature. These laws are designed to predict the performance of internal combustion engines (ICEs) based on parameters linked to their size. This approach is presented as an alternative to the extensive 0D/1D engine modeling techniques. Three distinct methodologies have been put forward: curve-fitted equations, the Willans line method and similitude analysis.

Curve-fitted equations vary from empirically derived scaling laws to those based on the fundamental engine performance parameters. Since the brake thermal efficiency and brake power output cannot be scaled based on the displacement volume only, the accuracy of the correlation needs to be estimated with the value of the coefficient of determination R^2, ranging from zero to one, with one indicating a perfect representation of the data by the model. The main advantage of the curve-fitted equations is their ease of implementation and their rapid results. The downsides are listed below.

1. A large data set is needed for engines with the same class (e.g., SI or CI, lean or stoichiometric, pre-chamber or open-chamber) and the same fuel type. This data set is currently missing for renewable fuels in large-bore SI engines.
2. No boundary conditions or constraints are defined on the scaling range. SI engines tend to be limited by abnormal combustion behavior, which is not included in this method.

To overcome these drawbacks, other methods were investigated as well. The Willans line method assumes that, for a constant engine speed, the fuel consumption and brake power/torque output increase linearly. Engine efficiency and frictional losses are parametrized as a function of the mean piston speed to represent one reference engine of a certain class. This parametrization can be used to represent any other engine of the same class with a different size. This method's advantages include its ease of implementation and the reliance on just one reference engine. The drawbacks are that, similarly to the curve-fitted equations, no boundary conditions are present to outline the scaling range. On top of that, this method is meant for right-scaling the ICE in hybrid electric vehicles, while it has not been validated for truly large differences in engine size.

The scaling laws based on the similitude analysis appear to be a better option. Under a predefined set of similarity conditions, this theory states that the dimensionless performance parameters of a scaled engine are identical to those of one optimized reference engine. The advantages of this method again include the reliance on just one reference engine and the fact that engine constraints such as the maximum mean piston speed, fuel injection pressure and engine speed are incorporated. The drawbacks of this method are as follows:

1. It presupposes identical dimensionless performance values, such as the BTE and BMEP, for scaled and reference engine, disregarding the advantages of a larger bore size. This limitation has been partially addressed by extending the similitude method with scaling laws based on the bore diameter ratio between the reference and scaled engines.

2. Deriving the requirements to achieve similitude is highly complex, and not all interaction effects are accounted for, leading to differences between the reference engine and the scaled engines.
3. While combustion similitude has been demonstrated for conventional diesel and, to some extent, for low-temperature combustion, it remains unproven for spark-ignition engines, with no guarantee that it can be established.

The possibility to prove combustion similitude for spark-ignition engines will be investigated in future work.

After evaluating these three scaling methods for the engine performance parameters with respect to the engine size, it is evident that in the short term, the most efficient approach to implement the BTE and brake power output values into ESOMs is through established curve-fitted equations. The high degree of correlation ($R^2 \geq 0.95$) suggests that a single power law does a good job in describing the scaling of power with displacement, regardless of the engine size or type. Efficiency, on the other hand, cannot be correlated effectively with engine size only ($R^2 \approx 0.74$). A higher accuracy can be achieved there by employing a data set of engines with the same or similar operating characteristics and engines dedicated to the same type of fuel. Integrating an arithmetic function for predicting the performance of small-to-large-scale conversion devices would also minimize the additional computation time compared to the implementation of 0D/1D or multi-dimensional modelling alternatives. The primary bottleneck, however, remains the lack of a comprehensive database of engines operating on alternative fuels. Although this limitation applies to the other two approaches as well, this method, in particular, would greatly benefit from an increased number of demonstration cases involving alternatively fueled SI ICEs. In the long term, the similitude approach may become a more robust method, but it will require time and effort to sequentially demonstrate the possibility of spark-ignited combustion similarity, to establish a universal scaling rule to achieve spark-ignited combustion similarity and, finally, to conduct numerous numerical simulations and experiments to validate the theory of spark-ignited combustion similarity.

Author Contributions: Conceptualization, W.S.; formal analysis, W.S.; writing—original draft preparation, W.S.; writing—review and editing, S.V.; supervision, S.V.; funding acquisition, S.V. All authors have read and agreed to the published version of the manuscript.

Funding: This research received no external funding.

Data Availability Statement: Not applicable.

Acknowledgments: The research reported in this paper was made possible by the support of the Energy Transition Fund of the Belgian federal government, within the project "Belgian Energy Transition", best-energy.be.

Conflicts of Interest: The authors declare no conflict of interest.

Appendix A

Curve-fitted equations based on Equations (9) and (12), respectively.

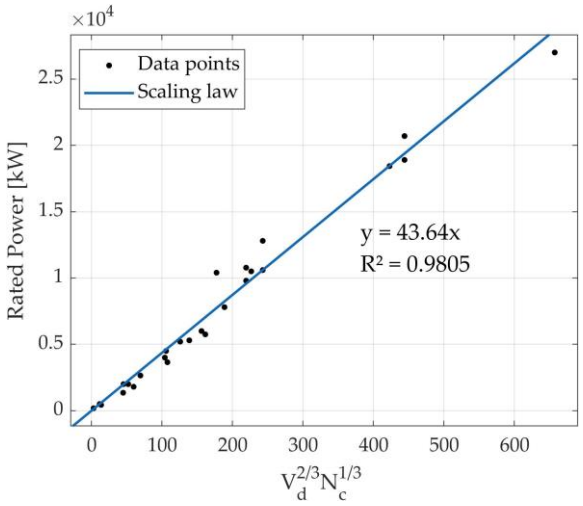

Figure A1. Linear relationship between rated power (kW) and $V_d^{\frac{2}{3}} N_c^{\frac{1}{3}}$.

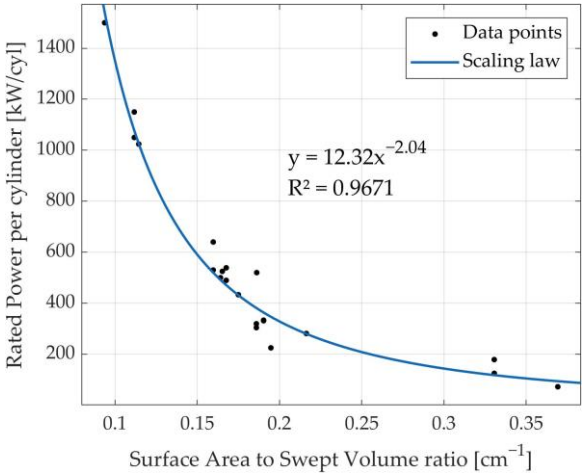

Figure A2. Rated cylinder power (kW/cyl) as a function of surface area to swept volume ratio (dm^{-1}). The correlation is based on Equation (12).

References

1. Shafiul Alam, M.; Al-Ismail, F.S.; Salem, A.; Abido, M.A. High-Level Penetration of Renewable Energy Sources into Grid Utility: Challenges and Solutions. *IEEE Access* **2020**, *8*, 190277–190299. [CrossRef]
2. Sorrenti, I.; Harild Rasmussen, T.B.; You, S.; Wu, Q. The Role of Power-to-X in Hybrid Renewable Energy Systems: A Comprehensive Review. *Renew. Sustain. Energy Rev.* **2022**, *165*, 112380. [CrossRef]
3. Samende, C.; Fan, Z.; Cao, J.; Fabián, R.; Baltas, G.N.; Rodriguez, P. Battery and Hydrogen Energy Storage Control in a Smart Energy Network with Flexible Energy Demand Using Deep Reinforcement Learning. *Energies* **2023**, *16*, 6770. [CrossRef]
4. Kebede, A.A.; Kalogiannis, T.; Van Mierlo, J.; Berecibar, M. A Comprehensive Review of Stationary Energy Storage Devices for Large Scale Renewable Energy Sources Grid Integration. *Renew. Sustain. Energy Rev.* **2022**, *159*, 112213. [CrossRef]
5. BloombergNEF. Available online: https://about.bnef.com/blog/energy-storage-investments-boom-battery-costs-halve-next-decade/#_ftn1 (accessed on 13 September 2022).
6. Heide, D.; von Bremen, L.; Greiner, M.; Hoffmann, C.; Speckmann, M.; Bofinger, S. Seasonal Optimal Mix of Wind and Solar Power in a Future, Highly Renewable Europe. *Renew. Energy* **2010**, *35*, 2483–2489. [CrossRef]
7. Heide, D.; Greiner, M.; von Bremen, L.; Hoffmann, C. Reduced Storage and Balancing Needs in a Fully Renewable European Power System with Excess Wind and Solar Power Generation. *Renew. Energy* **2011**, *36*, 2515–2523. [CrossRef]
8. Pleßmann, G.; Erdmann, M.; Hlusiak, M.; Breyer, C. Global Energy Storage Demand for a 100% Renewable Electricity Supply. *Energy Procedia* **2014**, *46*, 22–31. [CrossRef]
9. Feijoo, F.; Pfeifer, A.; Herc, L.; Groppi, D.; Duić, N. A Long-Term Capacity Investment and Operational Energy Planning Model with Power-to-X and Flexibility Technologies. *Renew. Sustain. Energy Rev.* **2022**, *167*, 112781. [CrossRef]
10. Brynolf, S.; Taljegard, M.; Grahn, M.; Hansson, J. Electrofuels for the Transport Sector: A Review of Production Costs. *Renew. Sustain. Energy Rev.* **2018**, *81*, 1887–1905. [CrossRef]

11. Rixhon, X.; Limpens, G.; Coppitters, D.; Jeanmart, H.; Contino, F. The Role of Electrofuels under Uncertainties for the Belgian Energy Transition. *Energies* **2021**, *14*, 4027. [CrossRef]
12. Plazas-Niño, F.A.; Ortiz-Pimiento, N.R.; Montes-Páez, E.G. National Energy System Optimization Modelling for Decarbonization Pathways Analysis: A Systematic Literature Review. *Renew. Sustain. Energy Rev.* **2022**, *162*, 112406. [CrossRef]
13. Dagoumas, A.S.; Koltsaklis, N.E. Review of Models for Integrating Renewable Energy in the Generation Expansion Planning. *Appl. Energy* **2019**, *242*, 1573–1587. [CrossRef]
14. Spataru, C.; Drummond, P.; Zafeiratou, E.; Barrett, M. Long-Term Scenarios for Reaching Climate Targets and Energy Security in UK. *Sustain. Cities Soc.* **2015**, *17*, 95–109. [CrossRef]
15. Aboumahboub, T.; Brecha, R.J.; Shrestha, H.B.; Fuentes, U.; Geiges, A.; Hare, W.; Schaeer, M.; Welder, L.; Gidden, M.J. Decarbonization of Australia s Energy System: Integrated Modeling of the Transformation of Electricity, Transportation, and Industrial Sectors. *Energies* **2020**, *13*, 3805. [CrossRef]
16. Limpens, G.; Jeanmart, H.; Maréchal, F. Belgian Energy Transition: What Are the Options? *Energies* **2020**, *13*, 261. [CrossRef]
17. Safonov, G.; Potashnikov, V.; Lugovoy, O.; Safonov, M.; Dorina, A.; Bolotov, A. The Low Carbon Development Options for Russia. *Clim. Change* **2020**, *162*, 1929–1945. [CrossRef]
18. Al Moussawi, H.; Fardoun, F.; Louahlia-Gualous, H. Review of Tri-Generation Technologies: Design Evaluation, Optimization, Decision-Making, and Selection Approach. *Energy Convers. Manag.* **2016**, *120*, 157–196. [CrossRef]
19. Perrone, D.; Castiglione, T.; Morrone, P.; Pantano, F.; Bova, S. Energetic, Economic and Environmental Performance Analysis of a Micro-Combined Cooling, Heating and Power (CCHP) System Based on Biomass Gasification. *Energies* **2023**, *16*, 6911. [CrossRef]
20. Jradi, M.; Riffat, S. Tri-Generation Systems: Energy Policies, Prime Movers, Cooling Technologies, Configurations and Operation Strategies. *Renew. Sustain. Energy Rev.* **2014**, *32*, 396–415. [CrossRef]
21. Badami, M.; Mura, M.; Campanile, P.; Anzioso, F. Design and Performance Evaluation of an Innovative Small Scale Combined Cycle Cogeneration System. *Energy* **2008**, *33*, 1264–1276. [CrossRef]
22. Montazerinejad, H.; Eicker, U. Recent Development of Heat and Power Generation Using Renewable Fuels: A Comprehensive Review. *Renew. Sustain. Energy Rev.* **2022**, *165*, 112578. [CrossRef]
23. Ren, F.; Wei, Z.; Zhai, X. A Review on the Integration and Optimization of Distributed Energy Systems. *Renew. Sustain. Energy Rev.* **2022**, *162*, 112440. [CrossRef]
24. Verhelst, S.; Sheppard, C.G.W. Multi-Zone Thermodynamic Modelling of Spark-Ignition Engine Combustion—An Overview. *Energy Convers. Manag.* **2009**, *50*, 1326–1335. [CrossRef]
25. Rakopoulos, C.D.; Michos, C.N.; Giakoumis, E.G. Availability Analysis of a Syngas Fueled Spark Ignition Engine Using a Multi-Zone Combustion Model. *Energy* **2008**, *33*, 1378–1398. [CrossRef]
26. D'Errico, G.; Cerri, T.; Pertusi, G. Multi-Objective Optimization of Internal Combustion Engine by Means of 1D Fluid-Dynamic Models. *Appl. Energy* **2011**, *88*, 767–777. [CrossRef]
27. Yun, K.T.; Cho, H.; Luck, R.; Mago, P.J. Modeling of Reciprocating Internal Combustion Engines for Power Generation and Heat Recovery. *Appl. Energy* **2013**, *102*, 327–335. [CrossRef]
28. Moret, S.; Codina Gironès, V.; Bierlaire, M.; Maréchal, F. Characterization of Input Uncertainties in Strategic Energy Planning Models. *Appl. Energy* **2017**, *202*, 597–617. [CrossRef]
29. Nguyen, D.; Kar, T.; Turner, J.W.G. Performance, Emissions, and Combustion Characteristics of a Hydrogen-Fueled Spark-Ignited Engine at Different Compression Ratios: Experimental and Numerical Investigation. *Energies* **2023**, *16*, 5730. [CrossRef]
30. Zhou, Y.; Hong, W.; Yang, Y.; Li, X.; Xie, F.; Su, Y. Experimental Investigation of Diluents Components on Performance and Emissions of a High Compression Ratio Methanol SI Engine. *Energies* **2019**, *12*, 3366. [CrossRef]
31. Falfari, S.; Cazzoli, G.; Mariani, V.; Bianchi, G.M. Hydrogen Application as a Fuel in Internal Combustion Engines. *Energies* **2023**, *16*, 2545. [CrossRef]
32. Yan, Y.; Liu, Z.; Liu, J. An Evaluation of the Conversion of Gasoline and Natural Gas Spark Ignition Engines to Ammonia/Hydrogen Operation from the Perspective of Laminar Flame Speed. *J. Energy Resour. Technol. Trans. ASME* **2023**, *145*, 012302. [CrossRef]
33. Yang, R.; Yan, Y.; Liu, Z.; Liu, J. *Formation and Evolution of Thermal and Fuel Nitrogen Oxides in the Turbulent Combustion Field of Ammonia Internal Combustion Engines*; SAE Technical Paper 2023-01-0192; SAE International: Warrendale, PA, USA, 2023.
34. Menon, S.; Cadou, C.P. *Scaling of Miniature Piston-Engine Performance, Part 1: Overall Engine Performance*; American Institute of Aeronautics and Astronautics, Inc.: Reston, VA, USA, 2013; Volume 29, pp. 774–787. [CrossRef]
35. Brown, S.; Menon, S.; Hagen, C. Investigation of Scaling Laws for Combustion Engine Performance. Available online: https://sites01.lsu.edu/faculty/smenon/wp-content/uploads/sites/133/2017/02/WSSCI_Provo_v5.pdf (accessed on 6 November 2023).
36. McMahon, T.A.; Bonner, J.T. *On Size and Life*; Scientific American Books: New York, NY, USA, 1983; Volume 1.
37. Muranaka, S.; Takagi, Y.; Ishida, T. *Factors Limiting the Improvement in Thermal Efficiency of S. I. Engine at Higher Compression Ratio*; SAE Technical Papers; SAE International: Warrendale, PA, USA, 1987; Volume 96, pp. 526–536. [CrossRef]
38. Arisawa, T.; Arai, T.; Sakane, Y.; Kobashi, Y.; Shibata, G.; Ogawa, H. CFD Analysis of Engine Size Dependence of Diesel Combustion. In Proceedings of the 27th ICE symposium of JSAE CDROM, Sapporo, Japan, 19–21 October 2016; pp. 19–21.
39. Chon, D.M.; Heywood, J.B. *Performance Scaling of Spark-Ignition Engines: Correlation and Historical Analysis of Production Engine Data*; SAE Technical Papers; SAE International: Warrendale, PA, USA, 2000. [CrossRef]

40. Heywood, J.B. *Internal Combustion Engine Fundamentals, McGraw-Hill Series in Mechanical Engineering*; MacGraw-Hill: New York, NY, USA, 1988.
41. Heywood, J.B.; Welling, O.Z. *Trends in Performance Characteristics of Modern Automobile SI and Diesel Engines*; SAE Technical Papers; SAE International: Warrendale, PA, USA, 2009; Volume 2, pp. 1650–1662. [CrossRef]
42. Rowton, A.K.; Ausserer, J.K.; Grinstead, K.D.; Litke, P.J.; Polanka, M.D. *Measuring Scaling Effects in Small Two-Stroke Internal Combustion Engines*; SAE Technical Papers; SAE International: Warrendale, PA, USA, 2014. [CrossRef]
43. Rowton, A.K. Measuring Scaling Effects in Small Two-Stroke Internal Combustion Engines. Master's Thesis, Department of the Air Force Air University, Montgomery, AL, USA, 2014.
44. Abidin, Z.; Hoag, K.; Badain, N. *Dilute Combustion Assessment in Large Bore, Low Speed Engines*; SAE Technical Papers; SAE International: Warrendale, PA, USA, 2017. [CrossRef]
45. Nork, D.B.; Fh, D.; Qriqra, A.; Kleuser, D.R. Deutz Hydrogen-ICE—A Simulation of the Entire System. In Proceedings of the 18th Symposium on Sustainable Mobility, Transport and Power Generation, Graz, Austria, 23–24 September 2021; pp. 150–161.
46. Sommermann, A.; Hinrichsen, F.; Malischewski, T.; Hyna, D.; Karl, C.; Schmitt, J.; Mcmackin, M.; Beck, H.; Truck, M.A.N.; Se, B. MAN H45 Hydrogen Engine: A Robust and Highly Efficient Technology for CO_2-Neutral Mobility. In Proceedings of the Symposium "Sustainable Mobility, Transport and Power Generation", Graz, Austria, 23–24 September 2021; pp. 162–176.
47. Thomas Koch, D.; Sousa, A.; Bertram, D. *H_2-Engine Operation with EGR Achieving High Power and High Efficiency Emission-Free Combustion*; SAE Technical Papers; SAE International: Warrendale, PA, USA, 2019. [CrossRef]
48. Ebert, T.; Koch, M.S.D.; Kerschl, B.S.D.; Fh, D.; Wehrli, M.; Vonnoe, M.E.M.; Lahni, M.S.T. Effectiveness of the H_2-Specific Operating Strategy in Dynamic Engine Operation. In Proceedings of the 18th Symposium on Sustainable Mobility, Transport and Power Generation, Graz, Austria, 23–24 September 2021; pp. 177–191.
49. Mahendar, S.K.; Larsson, T.; Erlandsson, A.C. Alcohol Lean Burn in Heavy Duty Engines: Achieving 25 Bar IMEP with High Efficiency in Spark Ignited Operation. *Int. J. Engine Res.* **2020**, *22*, 3313–3324. [CrossRef]
50. Li, X.; Zhen, X.; Xu, S.; Wang, Y.; Liu, D.; Tian, Z. Numerical Comparative Study on Knocking Combustion of High Compression Ratio Spark Ignition Engine Fueled with Methanol, Ethanol and Methane Based on Detailed Chemical Kinetics. *Fuel* **2021**, *306*, 121615. [CrossRef]
51. Brusstar, M.J.; Gray, C.L. *High Efficiency with Future Alcohol Fuels in a Stoichiometric Medium Duty Spark Ignition Engine*; SAE Technical Paper; SAE International: Warrendale, PA, USA, 2007; Volume 116, pp. 1183–1190. [CrossRef]
52. Kumar, G.S.; Kumar, G.E. Initial Development of a E85 Fueled, Multi Cylinder, Turbocharged, Spark Ignited, Heavy Duty Engine. *SAE Int. J. Engines* **2017**, *10*, 55–60. [CrossRef]
53. Ottosson, D.; Zioris, K. Experimental Comparison of DI and PFI in Terms of Emissions and Efficiency Running Ethanol-85. Master's Thesis, KTH Royal Institute of Technology, Stockholm, Sweden, 2014; p. 42.
54. Zhen, X.; Wang, Y.; Xu, S.; Zhu, Y. Numerical Analysis on Knock for a High Compression Ratio Spark-Ignition Methanol Engine. *Fuel* **2013**, *103*, 892–898. [CrossRef]
55. Zhen, X.; Wang, Y.; Xu, S.; Zhu, Y. Study of Knock in a High Compression Ratio Spark-Ignition Methanol Engine by Multi-Dimensional Simulation. *Energy* **2013**, *50*, 150–159. [CrossRef]
56. Zhen, X.; Wang, Y.; Zhu, Y. Study of Knock in a High Compression Ratio SI Methanol Engine Using Les with Detailed Chemical Kinetics. *Energy Convers. Manag.* **2013**, *75*, 523–531. [CrossRef]
57. Zhen, X.; Wang, Y. Study of Ignition in a High Compression Ratio SI (Spark Ignition) Methanol Engine Using LES (Large Eddy Simulation) with Detailed Chemical Kinetics. *Energy* **2013**, *59*, 549–558. [CrossRef]
58. Zhen, X.; Li, X.; Wang, Y.; Liu, D.; Tian, Z.; Wang, Y. Effects of the Initial Flame Kernel Radius and EGR Rate on the Performance, Combustion and Emission of High-Compression Spark-Ignition Methanol Engine. *Fuel* **2020**, *262*, 116633. [CrossRef]
59. Zhu, Z.; Gu, H.; Zhu, Z.; Wei, Y.; Zeng, K.; Liu, S. Investigation on Mixture Formation and Combustion Characteristics of a Heavy-Duty SI Methanol Engine. *Appl. Therm. Eng.* **2021**, *196*, 117258. [CrossRef]
60. Gong, C.; Liu, F.; Sun, J.; Wang, K. Effect of Compression Ratio on Performance and Emissions of a Stratified-Charge DISI (Direct Injection Spark Ignition) Methanol Engine. *Energy* **2016**, *96*, 166–175. [CrossRef]
61. Gong, C.; Yi, L.; Zhang, Z.; Sun, J.; Liu, F. Assessment of Ultra-Lean Burn Characteristics for a Stratified-Charge Direct-Injection Spark-Ignition Methanol Engine under Different High Compression Ratios. *Appl. Energy* **2020**, *261*, 114478. [CrossRef]
62. Björnestrand, L. Efficiency and Emission Analysis of a Methanol Fuelled Direct Injection Spark Ignition Heavy Duty Engine. Master's Thesis, Lunds Unversitet, Lund, Sweden, 2017.
63. Li, Y.; Bai, X.S.; Tunér, M.; Im, H.G.; Johansson, B. Investigation on a High-Stratified Direct Injection Spark Ignition (DISI) Engine Fueled with Methanol under a High Compression Ratio. *Appl. Therm. Eng.* **2019**, *148*, 352–362. [CrossRef]
64. Güdden, A.; Pischinger, S.; Geiger, J.; Heuser, B.; Müther, M. Methanol Combustion Systems for Heavy-Duty Applications: Diffusive or Premixed Combustion? In Proceedings of the 18th Symposium on Sustainable Mobility, Transport and Power Generation, Graz, Austria, 23–24 September 2021; pp. 38–51.
65. Bosklopper, J.J. Experimental and Simulation-Based Investigation of the Perfor-Mance of a 100% Methanol Port-Injected Spark-Ignited Engine. Master's Thesis, Delft University of Technology, Delft, The Netherlands, 2020.
66. Leng, X.; Deng, Y.; He, D.; Wei, S.; He, Z.; Wang, Q.; Long, W.; Zhu, S. A Preliminary Numerical Study on the Use of Methanol as a Mono-Fuel for a Large Bore Marine Engine. *Fuel* **2022**, *310*, 122309. [CrossRef]

67. Sturm, M.; Caterpillar, M. *CHP-Market Demand and Optimized Solutions with the Caterpillar G20CM34 10 MW Gas Engine*; Springer: Berlin/Heidelberg, Germany, 2019.
68. Loetz, A. Modeling and Measurement of Combustion and Emissions Formation in Gas Engine Pre-Chambers. In Proceedings of the CIMAC Congress, Vancouver, BC, Canada, 10–14 June 2019.
69. Burke, J. *Market Survey: 43rd Power Generation Order Survey*; Diesel & Gas Turbine Publications, Inc.: Waukesha, WI, USA, 2019.
70. Guido, C.; Napolitano, P.; Alfuso, S.; Corsetti, C.; Beatrice, C. How Engine Design Improvement Impacts on Particle Emissions from an HD SI Natural Gas Engine. *Energy* **2021**, *231*, 120748. [CrossRef]
71. Posada, F.; Chambliss, S.; Blumberg, K. Costs of Emission Reduction Technologies for Heavy-Duty Diesel Vehicles Acknowledgements. 2016. Available online: https://theicct.org/publication/costs-of-emission-reduction-technologies-for-heavy-duty-diesel-vehicles/ (accessed on 6 November 2023).
72. Ibrahim, A.; Bari, S. A Comparison between EGR and Lean-Burn Strategies Employed in a Natural Gas SI Engine Using a Two-Zone Combustion Model. *Energy Convers. Manag.* **2009**, *50*, 3129–3139. [CrossRef]
73. MAN; ROLLO E2842 Description of Engines. Available online: https://www.manrollo.com/wp-content/uploads/E2842-series.pdf (accessed on 30 March 2022).
74. McDowell, R.; Xiong, Y.; Zurlo, J.; Knudsen, J.; Donahue, R.; Feldner, M.; Youakim, M. Waukesha VHP Series Five Gas Engine: Increased Output, Reduced Operating Costs, Improved Component Cooling, and Updated Controls. In Proceedings of the CIMAC Congress, Vancouver, BC, Canada, 10–14 June 2019.
75. Wheeler, J.; Stein, J.; Hunter, G. Effects of Charge Motion, Compression Ratio, and Dilution on a Medium Duty Natural Gas Single Cylinder Research Engine. *SAE Int. J. Engines* **2014**, *7*, 1650–1664. [CrossRef]
76. Zhang, Q.; Li, M.; Li, G.; Shao, S.; Li, P. Transient Emission Characteristics of a Heavy-Duty Natural Gas Engine at Stoichiometric Operation with EGR and TWC. *Energy* **2017**, *132*, 225–237. [CrossRef]
77. Neame, G.R.; Gardiner, D.P.; Mallory, R.W.; Rao, V.K.; Bardon, M.F.; Battista, V. *Improving the Fuel Economy of Stoichiometrically Fuelled S.I. Engines by Means of EGR and Enhanced Ignition—A Comparison of Gasoline, Methanol and Natural Gas*; SAE Technical Papers; SAE International: Warrendale, PA, USA, 1995. [CrossRef]
78. Abd-Alla, G.H. Using Exhaust Gas Recirculation in Internal Combustion Engines: A Review. *Energy Convers. Manag.* **2002**, *43*, 1027–1042. [CrossRef]
79. Germane, G.J.; Wood, C.G.; Hess, C.C. *Lean Combustion in Spark-Ignited Internal Combustion Engines—A Review*; SAE Technical Papers; SAE International: Warrendale, PA, USA, 1983. [CrossRef]
80. Dunn-Rankin, D.; Therkelsen, P. *Lean Combustion: Technology and Control*; Springer: Berlin/Heidelberg, Germany, 2016; 267p.
81. Di Iorio, S.; Sementa, P.; Vaglieco, B.M. Experimental Investigation on the Combustion Process in a Spark Ignition Optically Accessible Engine Fueled with Methane/Hydrogen Blends. *Int. J. Hydrogen Energy* **2014**, *39*, 9809–9823. [CrossRef]
82. Wu, C.; Deng, K.; Wang, Z. The Effect of Combustion Chamber Shape on Cylinder Flow and Lean Combustion Process in a Large Bore Spark-Ignition CNG Engine. *J. Energy Inst.* **2016**, *89*, 240–247. [CrossRef]
83. Toulson, E.; Schock, H.J.; Attard, W.P. *A Review of Pre-Chamber Initiated Jet Ignition Combustion Systems*; SAE Technical Papers; SAE International: Warrendale, PA, USA, 2010. [CrossRef]
84. Shah, A.; Tunestal, P.; Johansson, B. Investigation of Performance and Emission Characteristics of a Heavy Duty Natural Gas Engine Operated with Pre-Chamber Spark Plug and Dilution with Excess Air and EGR. *SAE Int. J. Engines* **2012**, *5*, 1790–1801. [CrossRef]
85. Hlaing, P.; Echeverri Marquez, M.; Cenker, E.; Im, H.G.; Johansson, B.; Turner, J.W.G. Effects of Volume and Nozzle Area in Narrow-Throat Spark-Ignited Pre-Chamber Combustion Engines. *Fuel* **2022**, *313*, 123029. [CrossRef]
86. Kizuka, T.; Kawasaki, H.I. Development of Stable Combustion Technology for the World's Largest Bore Diameter Gas Engine. In Proceedings of the 29th CIMAC World Congress, Vancouver, BC, Canada, 10–14 June 2019.
87. Birgel, A.; Bowing, R.; Trapp, C.; Wimmer, A. GE's J920 Gas Engine—10.4 MW Power and More than 50% Electrical Efficiency. *MTZ Ind.* **2017**, *7*, 34–39. [CrossRef]
88. Solutions, M.E. MAN V35/44G. Available online: https://www.man-es.com/docs/default-source/document-sync/man-v35-44g-eng.pdf?sfvrsn=732fa54_0 (accessed on 17 March 2022).
89. Solutions, M.E. MAN V51/60G. Available online: https://www.man-es.com/docs/default-source/document-sync/man-v51-60g-eng.pdf?sfvrsn=3776bc19_0 (accessed on 17 March 2022).
90. Lauer, T. Impact of the Fuel Gas Quality on the Efficiency of a Large Gas Engine. In Proceedings of the 28th CIMAC World Congress, Helsinki, Finland, 6–10 June 2016.
91. Geiger, J. Combustion System Development for a Large Bore Gas Engine—Efficient Combination of Simulation and Experiment. In Proceedings of the 28th CIMAC World Congress, Helsinki, Finland, 2016., 6–10 June.
92. Issei, O. New Marine Gas Engine Development in YANMAR. In Proceedings of the 28th CIMAC World Congress, Helsinki, Finland, 6–10 June 2016.
93. Kuroiwa, T. Performance Improvement of Spark-Ignited Medium-Speed Gas Engine 28AGS. In Proceedings of the 29th CIMAC World Congress, Vancouver, BC, Canada, 10–14 June 2019.
94. Sakai, Y. Operational Experience and New Development for High Performance of Kawasaki Green Gas Engine. In Proceedings of the 28th CIMAC World Congress, Helsinki, Finland, 6–10 June 2016.

95. Yoshizumi, H. Improvement of Powser Generation Efficiency and Heat Recovery of Cooling Energy in Mitsubishi KU30GSI Gas Engine for Better Heat and Power Utilization. In Proceedings of the 28th CIMAC World Congress, Helsinki, Finland, 6–10 June 2016.
96. Wellander, R.; Rosell, J.; Richter, M.; Alden, M.; Andersson, O.; Johansson, B.; Duong, J.; Hyvonen, J. Study of the Early Flame Development in a Spark-Ignited Lean Burn Four-Stroke Large Bore Gas Engine by Fuel Tracer PLIF. *SAE Int. J. Engines* **2014**, *7*, 928–936. [CrossRef]
97. Wolfgramm, M. G20CM34—A Highly Flexible 10 MW Gas Engine Concept. In Proceedings of the 28th CIMAC World Congress, Helsinki, Finland, 6–10 June 2016.
98. Wideskog, M. Lean Burn Engines—The Optimal Power Source for Energy Solutions. In Proceedings of the 28th CIMAC World Congress, Helsinki, Finland, 6–10 June 2016.
99. Hlaing, P.; Echeverri Marquez, M.; Bhavani Shankar, V.S.; Cenker, E.; Ben Houidi, M.; Johansson, B. *A Study of Lean Burn Pre-Chamber Concept in a Heavy Duty Engine*; SAE Technical Papers; SAE International: Warrendale, PA, USA, 2019; pp. 1–13. [CrossRef]
100. Bondarenko, O. Gas Engine for Marine Application: Modelin and Control. In Proceedings of the 28th CIMAC World Congress, Helsinki, Finland, 6–10 June 2016.
101. Koda, K. Direct Measurement of Heat Loss on Combustion Chamber Wall in Gas Engine with Pre-Chamber. In Proceedings of the 29th CIMAC World Congress, Vancouver, BC, Canada, 10–14 June 2019.
102. Eicheldinger, S.; Bartkowski, T.; Schröder, A.; Prager, D.I.M.; Wachtmeister, P.D.I.G. *Experimental Investigation on the Influence of Brake Mean Effective Pressures Up to 30 Bar on the Behavior of a Large Bore Otto Gas Engine*; SAE Technical Papers; SAE International: Warrendale, PA, USA, 2019. [CrossRef]
103. Sander, U. MTU Series 4000 for Natural Gas Operation in Ships—Challenges for High Speed Gas Engines in Mobile Applications. In Proceedings of the 28th CIMAC World Congress, Helsinki, Finland, 6–10 June 2016.
104. Kunz, P. MTU Series 4000 for Natural Gas Operation in Ships—Challenges for High-Speed Gas Engines in Mobile Applications. In Proceedings of the 29th CIMAC World Congress, Vancouver, BC, Canada, 10–14 June 2019.
105. Caterpillar PRODUCTSPECIFICATIES VOOR CG260-16. Available online: https://www.cat.com/nl_NL/products/new/power-systems/electric-power/gas-generator-sets/15969827.html (accessed on 17 March 2022).
106. Wärtsilä Wärtsilä 34SG BALANCER. Available online: https://www.wartsila.com/docs/default-source/power-plants-documents/downloads/product-leaflets/w34sg-balancer-leaflet.pdf?utm_term=energy&utm_content=leaflet (accessed on 17 March 2022).
107. Wärtsilä WÄRTSILÄ 34SG GAS ENGINE GENERATING SET. Available online: https://www.wartsila.com/docs/default-source/power-plants-documents/downloads/product-leaflets/w34sg_leaflet.pdf (accessed on 17 March 2022).
108. Wärtsilä WÄRTSILÄ 50SG GAS ENGINE GENERATING SET. Available online: https://www.wartsila.com/docs/default-source/power-plants-documents/downloads/product-leaflets/w50sg_leaflet.pdf (accessed on 17 March 2022).
109. Urlaub, A. *Verbrennungsmotoren*; Springer: Berlin/Heidelberg, Germany, 1995.
110. Rizzoni, G.; Guzzella, L.; Baumann, B.M. Unified Modeling of Hybrid Electric Vehicle Drivetrains. *IEEE/ASME Trans. Mechatron.* **1999**, *4*, 246–257. [CrossRef]
111. Sundström, O.; Guzzella, L.; Soltic, P. Torque-Assist Hybrid Electric Powertrain Sizing: From Optimal Control towards a Sizing Law. *IEEE Trans. Control. Syst. Technol.* **2010**, *18*, 837–849. [CrossRef]
112. Verhaeghe, E. *Optimization of Hybrid Electric Vehicles Based on Fuel Consumption*; Ghent University: Gent, Belgium, 2014.
113. Ebbesen, S.; Elbert, P.; Guzzella, L. Engine Downsizing and Electric Hybridization Under Consideration of Cost and Drivability. *Oil Gas Sci. Technol.–Rev. D'ifp Energ. Nouv.* **2013**, *68*, 109–116. [CrossRef]
114. Sorrentino, M.; Mauramati, F.; Arsie, I.; Cricchio, A.; Pianese, C.; Nesci, W. *Application of Willans Line Method for Internal Combustion Engines Scalability towards the Design and Optimization of Eco-Innovation Solutions*; SAE Technical Papers; SAE International: Warrendale, PA, USA, 2015. [CrossRef]
115. Davey, K.; Darvizeh, R.; Golbaf, A.; Sadeghi, H. The Breaking of Geometric Similarity. *Int. J. Mech. Sci.* **2020**, *187*, 105925. [CrossRef]
116. Coutinho, C.P.; Baptista, A.J.; Dias Rodrigues, J. Reduced Scale Models Based on Similitude Theory: A Review up to 2015. *Eng. Struct.* **2016**, *119*, 81–94. [CrossRef]
117. Lanchester, F.W. The Horse-Power of the Petrol Motor in Its Relation to Bore, Stroke and Weight. *Proc. Inst. Automob. Eng.* **2006**, *1*, 153–220. [CrossRef]
118. Chikahisa, T.; Murayama, T. Theory on Combustion Similarity for Different-Sized Diesel Engines. *JSME Int. J.* **1990**, *33*, 395–400. [CrossRef]
119. Zhou, X.; Li, T.; Lai, Z.; Wang, B. *Theoretical Study on Similarity of Diesel Combustion*; SAE Technical Paper; SAE International: Warrendale, PA, USA, 2018; Volume 39, pp. 1–7. [CrossRef]
120. Chikahisa, T.; Kikuta, K.; Murayama, T. *Combustion Similarity for Different Size Diesel Engines: Theoretical Prediction and Experimental Results*; SAE Technical Papers; SAE International: Warrendale, PA, USA, 1992; Volume 101, pp. 780–789. [CrossRef]
121. Bergin, M.J.; Hessel, R.P.; Reitz, R.D. *Optimization of a Large Diesel Engine via Spin Spray Combustion*; SAE Technical Papers; SAE International: Warrendale, PA, USA, 2005; Volume 114, pp. 765–779. [CrossRef]
122. Stager, L.A.; Reitz, R.D. *Assessment of Diesel Engine Size-Scaling Relationships*; SAE Technical Papers; SAE International: Warrendale, PA, USA, 2007; Volume 2007, pp. 776–790. [CrossRef]

123. Pickett, L.M.; Siebers, D.L.; Idicheria, C.A. *Relationship between Ignition Processes and the Lift-Off Length of Diesel Fuel Jets*; SAE Technical Papers; SAE International: Warrendale, PA, USA, 2005. [CrossRef]
124. Zhou, X.; Li, T.; Yi, P. The Similarity Ratio Effects in Design of Scaled Model Experiments for Marine Diesel Engines. *Energy* **2021**, *231*, 121116. [CrossRef]
125. Shi, Y.; Reitz, R.D. *Study of Diesel Engine Size-Scaling Relationships Based on Turbulence and Chemistry Scales*; SAE Technical Papers; SAE International: Warrendale, PA, USA, 2008. [CrossRef]
126. Staples, L.R.; Reitz, R.D.; Hergart, C. *An Experimental Investigation into Diesel Engine Size-Scaling Parameters*; SAE Technical Papers; SAE International: Warrendale, PA, USA, 2009; pp. 1068–1084. [CrossRef]
127. Lee, C.W.; Reitz, R.D.; Kurtz, E. A Numerical Study on Diesel Engine Size-Scaling in Low Temperature Combustion Operation. *Numeri. Heat Transf. A Appl.* **2010**, *58*, 681–701. [CrossRef]
128. Zhou, X.; Li, T.; Wei, Y.; Wu, S. Scaling Spray Combustion Processes in Marine Low-Speed Diesel Engines. *Fuel* **2019**, *258*, 116133. [CrossRef]
129. Tess, M.J.; Lee, C.W.; Reitz, R.D. Diesel Engine Size Scaling at Medium Load without EGR. *SAE Int. J. Engines* **2011**, *4*, 1993–2009. [CrossRef]
130. Chuahy, F.D.F.; Olk, J.; DelVescovo, D.; Kokjohn, S.L. An Engine Size–Scaling Method for Kinetically Controlled Combustion Strategies. *Int. J. Engine Res.* **2020**, *21*, 927–947. [CrossRef]
131. Shi, Y.; Ge, H.-W.; Reitz, R.D. *Computational Optimization of Internal Combustion Engines*; Springer Science & Business Media: Berlin, Germany, 2011. [CrossRef]
132. Livengood, J.C.; Wu, P.C. Correlation of Autoignition Phenomena in Internal Combustion Engines and Rapid Compression Machines. *Symp. (Int.) Combust.* **1955**, *5*, 347–356. [CrossRef]